



HAL
open science

Total Energy beyond GW: Exact Results and Guidelines for Approximations

Abdallah El-Sahili, Francesco Sottile, Lucia Reining

► **To cite this version:**

Abdallah El-Sahili, Francesco Sottile, Lucia Reining. Total Energy beyond GW: Exact Results and Guidelines for Approximations. *Journal of Chemical Theory and Computation*, 2024, 20 (5), pp.1972-1987. 10.1021/acs.jctc.3c01200 . hal-04794326

HAL Id: hal-04794326

<https://hal.science/hal-04794326v1>

Submitted on 20 Nov 2024

HAL is a multi-disciplinary open access archive for the deposit and dissemination of scientific research documents, whether they are published or not. The documents may come from teaching and research institutions in France or abroad, or from public or private research centers.

L'archive ouverte pluridisciplinaire **HAL**, est destinée au dépôt et à la diffusion de documents scientifiques de niveau recherche, publiés ou non, émanant des établissements d'enseignement et de recherche français ou étrangers, des laboratoires publics ou privés.

Total energy beyond GW : exact results and guidelines for approximations

Abdallah El-Sahili,^{*,†,‡} Francesco Sottile,^{†,‡} and Lucia Reining^{†,‡}

[†]*LSI, CNRS, CEA/DRF/IRAMIS, École Polytechnique, Institut Polytechnique de Paris,
F-91120 Palaiseau, France*

[‡]*European Theoretical Spectroscopy Facility (ETSF)*

E-mail: abdallah.el-sahili@polytechnique.edu

December 8, 2023

Abstract

The total energy and electron addition and removal spectra can in principle be obtained exactly from the one-body Green's function. In practice, the Green's function is obtained from an approximate self-energy. In the framework of many-body perturbation theory, we derive different expressions that are based on an approximate self-energy, but that yield nevertheless in principle the exact exchange-correlation contribution to the total energy for any interaction strength. Response functions play a crucial role, which explains why, for example, ingredients from time-dependent density functional theory can be used to build these approximate self-energies. We show that the key requirement for obtaining exact results is the consistent combination of ingredients. Also when further approximations are made, as it is necessary in practice, this consistency remains the key to obtain good results. All findings are illustrated using the exactly solvable symmetric Hubbard dimer.

1 Introduction

Many important properties of materials are linked to observables that can be expressed in principle as expectation values in the many-body ground state or in thermal equilibrium. In practice, the use of many-body wavefunctions is often avoided by rather describing the observables as functionals of more compact quantities, i.e., quantities that depend on less arguments, such as the density¹, one-body reduced density matrix²⁻⁴, or one- or two-body Green's functions⁵. This represents a trade-off: often, one does not know the exact functional for an observable in terms of these quantities, and approximations have to be designed. One important example is the total energy: it can be straightforwardly formulated in terms of the one-body Green's function (GF)⁶, whereas no exact explicit expression in terms of the density is known. The same holds for electron addition and removal spectral functions. Excitation spectra involving neutral excitations in linear response, instead, are easily expressed in terms of a two-body Green's function, but not in terms of the ground state density or the one-body Green's function⁵. Even when the expressions are known, one faces another problem: while the use of the compact quantities carries the promise of reduced computational load, they are themselves only known explicitly as expectation values involving many-body wavefunctions. Therefore, nothing is gained, unless one finds ways to calculate them in a different way, which may be in principle exact, and in practice, require approximations. Typically, the density is obtained from the Kohn-Sham equations⁷ with an approximate exchange-correlation (xc) potential, and the GF, from a Dyson equation with an approximate xc self-energy Σ_{xc} ⁸. It is therefore not always obvious which framework (Density Functional Theory (DFT), Green's Function Functional Theory, etc.) is the best choice to access a given observable.

This holds in particular for the total ground state energy E_0 . While the Galitskii-Migdal formula⁶ or functional expressions such as the Luttinger-Ward⁹ or Klein¹⁰ functionals yield an in principal exact and, in the latter two cases, even variational, form in terms of the Green's function G , the need for approximations to the GF itself strongly impacts the quality of the results. Together with a computational load far heavier than that of the most

widely used density functionals, this explains why the vast majority of total energy calculations is performed using DFT, not Green's functions. Still, research concerning total energy calculations using Green's functions is active and important¹¹⁻¹⁴. Besides the - important - fact that in principle expressions for E_0 as functional of G and/or Σ_{xc} are known, the Green's functions framework benefits from the existence of powerful approximations. In particular, Many-Body Perturbation Theory (MBPT)⁸ suggests a way to expand the self-energy in diagrams that carry physical meaning and that are therefore helpful to describe phenomena such as the van der Waals dispersion interaction¹⁵. For situations that show only weak to moderate interaction effects, MBPT is often considered to be a systematic way to proceed, although in practice renormalizations, such as screening of the Coulomb interaction, are needed. In particular, even the lowest order of an expansion of the self-energy in terms of the screened Coulomb interaction W , which is the widely used GW approximation¹⁶, has been very successful for the calculation of the quasi-particle (QP) part of electron addition and removal spectra in finite and extended systems^{5,17-24}.

However, there are many cases where the GW approximation is not sufficient. On one hand, the description of QP energies is not always good and certainly worsens in more strongly correlated systems^{5,25}. On the other hand, other quantities, such as satellite features in the electron addition and removal spectra, are often less well described, even in absence of strong correlation^{26,27}. Most importantly, GW does not necessarily yield total energies of better quality than currently used density functionals^{13,14,28}. Research on total energies in terms of GFs goes therefore hand in hand with research on approximations to the self-energy beyond GW . The most straightforward way to go would be to explore higher orders in W , and important research in this direction is ongoing²⁹⁻³⁹. In many cases it cannot, however, bring a practical solution, since the resulting expressions become quickly very cumbersome and costly, and since perturbation theory will diverge when the interaction is too strong. Therefore, it would be desirable to find an efficient way to terminate the perturbation series.

In the various possible ways to express the xc energy contribution to the total energy

such as using the adiabatic connection fluctuation dissipation theorem^{40,41}, the polarizability plays a key role. This suggests to explore links to other frameworks that are used to access the polarizability, in particular, Time-Dependent DFT (TDDFT)⁴². Indeed, there is a long, and sometimes very successful, history of attempts to use TDDFT in order to go beyond GW in terms of vertex corrections based on the xc kernel f_{xc} ^{43–54}, the functional derivative with respect to the density of the xc potential v_{xc} of TDDFT⁵⁵, or related linear response kernels that may be closer to the many-body Green’s functions framework^{56–59}. This kind of combination leads to the so-called $G\tilde{W}$ self-energy, where the Coulomb interaction is screened by a test charge-test electron (TCTE) dielectric function instead of the test charge-test charge (TCTC) one used in the GW approximation^{60,61}. Independently of the specific recipe that is used in the various $G\tilde{W}$ expressions, these approaches replace the complicated exact vertex function Γ that depends on three space, spin and time arguments by a two-arguments function $(1 - f_{xc}\chi_0)^{-1}$, where χ_0 is an independent-particle polarizability. Therefore, the resulting self-energy is always approximate⁴⁹. Nevertheless, using a $G\tilde{W}$ self-energy instead of GW often improves the QP energies^{43,52,54}. At the same time, the idea is much less explored when it comes to total energies^{52,62}. Moreover, to the best of our knowledge a systematic study for both total energy and spectra that would discern the effect of the replacement of the full Γ by a two-arguments vertex on one side, from the effect of approximations to the f_{xc} itself on the other side, is still missing.

The present work has a focus on the total xc energy, while making a link to other aspects of the GF when interesting. It addresses the following questions: *Could a self-energy with a two-arguments vertex correction, and in particular, a TDDFT-derived one, yield in principle exact results? If yes, how do we have to build the corresponding expressions for the total xc energy? How do widely used approximations impact the results? And what happens to the kinetic energy and to spectra?* As we will show, there are indeed different possibilities to obtain in principle exact expressions for the total xc energy, which are moreover quite robust when widely used approximations are made. Consistent combination of ingredients

is a key requirement for this to be true. With these self-energies, the kinetic energy is not exact in principle, but we examine the possibility to use the virial theorem in order to overcome this issue. This allows us moreover to make an interesting comparison to the widely used adiabatic connection approach, which also makes use of the polarizability, but without involving a self-energy. Spectra are also approximate in principle when a two-arguments vertex correction is used, but we find that the $G\tilde{W}$ results still exhibit improvements over GW .

Our investigation and discussion is general, and it is accompanied by an illustration using the exactly solvable symmetric Hubbard dimer at half-filling. The paper is organized as follows: the theoretical background is given in Sec. 2. Theoretical developments made on this basis are presented and discussed in Sec. 3. The results for the Hubbard dimer are contained in Sec. 4. Conclusions are summarized in Sec. 5.

2 Theoretical background

2.1 Total energy and spectral function in terms of the GF

The ground state total energy E_0 can be expressed in terms of the time ordered GF^{6,13}

$$\begin{aligned}
 E_0 = & \underbrace{-i \lim_{t_2 \rightarrow t_1^+} \int dx_1 \left[-\frac{\nabla_{r_1}^2}{2} + v_{\text{ext}}(x_1) \right] G(x_1, x_1; t_1 - t_2)}_{E_{\text{k}} + E_{\text{ext}}} \\
 & \underbrace{-\frac{i}{2} \lim_{t_2 \rightarrow t_1^+} \int dx_1 v_{\text{H}}(x_1) G(x_1, x_1; t_1 - t_2)}_{E_{\text{H}}} \\
 & \underbrace{-\frac{i}{2} \lim_{t_2 \rightarrow t_1^{++}} \int dx_1 dx_3 dt_3 \Sigma_{\text{xc}}(x_1, x_3; t_1 - t_3) G(x_3, x_1; t_3 - t_2)}_{E_{\text{xc}}}, \quad (1)
 \end{aligned}$$

where $x = (r, \sigma)$ stands for position and spin, and $t^+ \equiv \lim_{\eta \rightarrow 0^+} (t + \eta)$. Here, we have highlighted the different contributions to the total energy, namely the kinetic energy E_{k} , the contribution

E_{ext} coming from the external potential v_{ext} , the Hartree energy E_{H} given in terms of the Hartree potential v_{H} , and the exchange-correlation energy E_{xc} expressed in terms of the exchange-correlation self-energy Σ_{xc} . The last two terms compose the interaction energy $E^{\text{inter}} \equiv E_{\text{H}} + E_{\text{xc}}$. Note that here, in the context of MBPT, E_{xc} refers specifically to the exchange-correlation energy of the Coulomb interaction, in contrast to the DFT framework where the xc energy also includes the correlation contribution from the kinetic energy. The specific form Eq. (1) of the Galitskii-Migdal equation is convenient in order to discuss separately the different contributions to the total energy, and to find specific improvements for each part. While such a strategy does not benefit from error canceling and therefore does not necessarily lead to globally improved results, it helps to obtain deeper insight, and eventually to arrive to the good result for the good reason.

The main quantity of interest is Σ_{xc} , which can be expressed exactly as

$$\Sigma_{\text{xc}}(1, 2) = i \int d(34) G(1, 4) W(3, 1^+) \Gamma(4, 2, 3), \quad (2)$$

where $1 = (x_1, t_1) = (r_1, \sigma_1, t_1)$ stands for position, spin and time. The screened Coulomb interaction W is given by

$$W(1, 2) = v_c(1, 2) + \int d(34) v_c(1, 3) \chi(3, 4) v_c(4, 2), \quad (3)$$

with v_c the bare Coulomb interaction $v_c(1, 2) = \delta(t_1 - t_2) \frac{1}{|r_1 - r_2|}$ and χ the reducible polarizability. The main complication stems from the vertex function Γ , defined as

$$\Gamma(4, 2, 3) = \delta(4, 3) \delta(2, 3) + \frac{\delta \Sigma_{\text{xc}}(4, 2)}{\delta v_{\text{cl}}(3^{++}, 3^+)}, \quad (4)$$

where $v_{\text{cl}} = v_{\text{H}} + v_{\text{ext}}$ is the total classical potential. Since Γ is in turn determined by the self-energy, in most cases it cannot be expressed in a closed form nor calculated exactly. To lowest order in the Coulomb interaction $\Gamma(4, 2, 3) \approx \delta(4, 3) \delta(2, 3)$. Corrections to this result are

called vertex corrections. Neglecting vertex corrections one obtains the GW approximation, where $\Sigma_{\text{xc}}(1, 2) = iG(1, 2)W(2, 1^+)$ ¹⁶.

Once the self-energy is determined in the chosen approximation, the GF is obtained by solving the Dyson equation

$$G(1, 2) = G_0(1, 2) + \int d(34) G_0(1, 3) \left(v_{\text{H}}(3, 4) + \Sigma_{\text{xc}}(3, 4) \right) G(4, 2), \quad (5)$$

where G_0 is the non-interacting GF. Finally, the resulting GF can be used to calculate E_0 from Eq. (1) or to evaluate the spectral function from the frequency Fourier transform of G ,

$$A(x, x, \omega) = \frac{1}{\pi} |\text{Im}(G(x, x; \omega))|. \quad (6)$$

2.2 Interaction energy in terms of the polarizability

Our focus is to find accurate expressions for the interaction energy E^{inter} . For this purpose, it is useful to express it in terms of the reducible polarizability χ ⁶².

For a system with N electrons in its ground state, the interaction energy is given by the expectation value of the Coulomb interaction operator \hat{V} in the many-body ground state $|N_0\rangle$,

$$E^{\text{inter}} = \langle N_0 | \hat{V} | N_0 \rangle = \frac{1}{2} \int dx_1 dx_2 v_c(x_1, x_2) \langle N_0 | \hat{\psi}^\dagger(x_2) \hat{\psi}^\dagger(x_1) \hat{\psi}(x_1) \hat{\psi}(x_2) | N_0 \rangle, \quad (7)$$

where $\hat{\psi}$ and $\hat{\psi}^\dagger$ are the annihilation and creation field operators, respectively. On the other hand, the reducible polarizability χ is defined as

$$\begin{aligned} \chi(x_1, t_1; x_2, t_2) = & -iG(x_1, t_1; x_1, t_1^+)G(x_2, t_2; x_2, t_2^+) \\ & - i \langle N_0 | \hat{T}[\hat{\psi}^\dagger(x_1, t_1^+) \hat{\psi}(x_1, t_1) \hat{\psi}^\dagger(x_2, t_2^+) \hat{\psi}(x_2, t_2)] | N_0 \rangle. \end{aligned} \quad (8)$$

In the limit $t_2 = t_1^{++}$,

$$\begin{aligned}
\chi(x_1, t_1; x_2, t_1^{++}) &= -iG(x_1, t_1; x_1, t_1^+)G(x_2, t_1^{++}; x_2, t_1^{+++}) \\
&\quad - i \langle N_0 | \hat{\psi}^\dagger(x_2) \hat{\psi}(x_1) | N_0 \rangle \delta(x_2 - x_1) - i \langle N_0 | \hat{\psi}^\dagger(x_2) \hat{\psi}^\dagger(x_1) \hat{\psi}(x_1) \hat{\psi}(x_2) | N_0 \rangle \\
&\quad = i n(x_1) n(x_2) - i \rho(x_1, x_2) \delta(x_2 - x_1) - i \langle N_0 | \hat{\psi}^\dagger(x_2) \hat{\psi}^\dagger(x_1) \hat{\psi}(x_1) \hat{\psi}(x_2) | N_0 \rangle, \quad (9)
\end{aligned}$$

where we used the anticommutation relation $\{\psi(x_2), \psi^\dagger(x_1)\} = \delta(x_2 - x_1)$, and where we introduced the one-body reduced density-matrix $\rho(x_1, x_2) = \langle N_0 | \hat{\psi}^\dagger(x_2) \hat{\psi}(x_1) | N_0 \rangle = -iG(x_1, t, x_2, t^+)$, with the electron density $n(x_1) = \rho(x_1, x_1)$. The last term in Eq. (9) enters the definition of the interaction energy in Eq. (7). The interaction energy can therefore be expressed in terms of the polarizability χ as

$$\begin{aligned}
E^{\text{inter}} &= \frac{1}{2} \int dx_1 dx_2 v_c(x_1, x_2) n(x_1) n(x_2) \\
&\quad + \frac{i}{2} \int dx_1 dx_2 v_c(x_1, x_2) \chi(x_1, t_1; x_2, t_1^{++}) - \frac{1}{2} \int dx_1 dx_2 v_c(x_1, x_2) \rho(x_1, x_2) \delta(x_2 - x_1), \quad (10)
\end{aligned}$$

where the first term is the Hartree energy and the last two terms are the exchange-correlation energy. This formulation of E_{xc} is not directly suitable for practical purposes, since it consists of terms containing a divergence that cancels in the sum. It is, however, a good starting point for the developments in the next section.

3 Theoretical developments

3.1 A freedom of choice

In order to eliminate the problematic last term in Eq. (10), we introduce a generalized independent-particle polarizability defined as $\chi_0(1, 2) \equiv -i\bar{G}(1, 2^+) \bar{G}(\bar{2}, 1^+)$. Its time diag-

onal is

$$\chi_0(x_1, t, x_2, t^{++}) = -i\bar{G}(x_1, t; x_2, t^{+++})\bar{G}(x_2, t^{++}; x_1, t^+) \quad (11)$$

$$= \bar{\rho}(x_1, x_2) \left(-i \langle \bar{N}_0 | \hat{\psi}(x_2) \hat{\psi}^\dagger(x_1) | \bar{N}_0 \rangle \right) \quad (12)$$

$$= -i\bar{\rho}(x_1, x_2) \langle \bar{N}_0 | \delta(x_2 - x_1) - \hat{\psi}^\dagger(x_1) \hat{\psi}(x_2) | \bar{N}_0 \rangle \quad (13)$$

$$= -i\bar{\rho}(x_1, x_2) \delta(x_2 - x_1) + i\bar{\rho}(x_1, x_2) \bar{\rho}(x_2, x_1), \quad (14)$$

where $|\bar{N}_0\rangle$ is the many-body ground state corresponding to a system that could be the true interacting system or an auxiliary interacting or non-interacting system. \bar{G} and $\bar{\rho}$ are the corresponding GF and the corresponding density matrix, respectively.

In the last term of Eq. (10), only the diagonal of the density matrix is needed. In order to replace this term, we can therefore consider all systems that yield the exact density $\bar{\rho}(x, x) = n(x)$, such as the true interacting system, or the Kohn-Sham auxiliary system. This leaves considerable freedom, which we can use to derive different exact expressions for E^{inter} and to design efficient approximations. Indeed, when $\bar{\rho}(x, x) = n(x)$ we have, from Eq. (14)

$$n(x_1) \delta(x_2 - x_1) = i\chi_0(x_1, t; x_2, t^{++}) + \bar{\rho}(x_1, x_2) \bar{\rho}(x_2, x_1), \quad (15)$$

which, replaced in Eq. (10), yields

$$E_{\text{xc}} = -\frac{1}{2} \int dx_1 dx_2 v_c(x_1, x_2) \bar{\rho}(x_1, x_2) \bar{\rho}(x_2, x_1) \quad (16)$$

$$+ \frac{i}{2} \int dx_1 dx_2 v_c(x_1, x_2) \left(\chi(x_1, t_1; x_2, t_1^{++}) - \chi_0(x_1, t_1; x_2, t_1^{++}) \right) \\ = \bar{E}_x + \bar{E}_c = \bar{E}_x + E_c + (E_x - \bar{E}_x). \quad (17)$$

The first term in Eq. (16) is \bar{E}_x , the exchange energy corresponding to $|\bar{N}_0\rangle$. Since the derivation shows that the sum of all terms is the exact exchange-correlation energy, the second term in Eq. (16) \bar{E}_c contains the exact correlation energy plus a correction that

compensates the error of \bar{E}_x with respect to the exact exchange energy E_x . *It is crucial to note that one can use any system defined by a ground state $|\bar{N}_0\rangle$, as long as this system yields the exact density: this will yield the exact Coulomb interaction energy, although $\bar{\rho}$ is not the density matrix of the true interacting system.* Two most obvious choices are either the true many-body (MB) system with $\bar{G} = G$, which leads to $\chi_0^{\text{MB}} \rightarrow -iGG$ and $\bar{\rho}(x_1, x_2) = \rho(x_1, x_2)$ the true density matrix, or the Kohn-Sham (KS) system with $\chi_0 \rightarrow \chi_0^{\text{KS}} \equiv -iG^{\text{KS}}G^{\text{KS}}$ the independent-particle polarizability built with the Kohn-Sham Green's function, and $\bar{\rho} \rightarrow \rho^{\text{KS}}$ the KS density matrix.

3.2 Exact exchange-correlation energy from approximate self-energies

Our next goal is to make a self-energy appear in the expression of E_{xc} . To this aim, we rewrite Eq. (16) as

$$E_{\text{xc}} = \frac{1}{2} \int dx_1 d2 \bar{G}(1, 2^+) \bar{G}(2, 1^+) v_c(2, 1) + \frac{i}{2} \int dx_1 d3 v_c(3, 1) [\chi(1, 3^{++}) - \chi_0(1, 3^{++})] \quad (18)$$

$$= \frac{1}{2} \int dx_1 d2 \bar{G}(1, 2^+) \bar{G}(2, 1^+) v_c(2, 1) \quad (19)$$

$$+ \frac{i}{2} \int dx_1 (234) \chi_0(1, 2) [v_c(2, 4) + \bar{f}_{\text{xc}}(2, 4)] \chi(4, 3^{++}) v_c(3, 1),$$

where we have introduced the generalized exchange-correlation kernel \bar{f}_{xc} that, once a choice for χ_0 is made, is defined from the Dyson-like equation

$$\chi(1, 2) = \chi_0(1, 2) + \int d(34) \chi_0(1, 3) \left(v_c(3, 4) + \bar{f}_{\text{xc}}(3, 4) \right) \chi(4, 2), \quad (20)$$

keeping in mind that χ is always the exact reducible polarizability. When χ_0 is chosen to be the KS independent particle polarizability, $\bar{f}_{\text{xc}} = f_{\text{xc}}$, the xc kernel of linear response

TDDFT⁵⁵, but, as pointed out above, other choices are possible.¹ By using the definition of χ_0 , given in the beginning of 3.1, Eq. (19) can be written as

$$E_{\text{xc}} = \int dx_1 d2 \bar{G}(1, 2^+) \bar{G}(2, 1^+) \left(v_c(2, 1) + \int d(34) (v_c(2, 4) + \bar{f}_{\text{xc}}(2, 4)) \chi(4, 3^{++}) v_c(3, 1) \right) \quad (21)$$

$$= \int dx_1 d2 \bar{G}(1, 2) \bar{G}(2, 1^{++}) \left(v_c(2, 1^+) + \int d(34) (v_c(2, 4) + \bar{f}_{\text{xc}}(2, 4)) \chi(4, 3^{++}) v_c(3, 1^+) \right) \quad (22)$$

$$= \frac{1}{2} \int dx_1 d2 \bar{G}(1, 2) \bar{W}(2, 1^+) \bar{G}(2, 1^{++}), \quad (23)$$

where we have defined the generalized TCTE screened Coulomb interaction²

$$\bar{W}(2, 1) = v_c(2, 1) + \int d(34) \left(v_c(2, 4) + \bar{f}_{\text{xc}}(1, 4) \right) \chi(4, 3^{++}) v_c(3, 1). \quad (24)$$

In this way, the *exact* exchange-correlation energy takes a form analogous to the last term in the Galitskii-Migdal expression Eq. (1):

$$E_{\text{xc}} = -\frac{i}{2} \int dx_1 d2 \bar{\Sigma}_{\text{xc}}(1, 2) \bar{G}(2, 1^{++}), \quad (25)$$

with an exchange-correlation self-energy

$$\bar{\Sigma}_{\text{xc}}(1, 2) \equiv i \bar{G}(1, 2) \bar{W}(2, 1^+). \quad (26)$$

The important point to stress here is the fact that the *exact* E_{xc} is obtained with an *approximate* self-energy Eq. (26). This approximation is often called $G\tilde{W}$. It is usually derived⁴³ by replacing $\Sigma_{\text{xc}}(4, 2)$ in the functional derivative in Eq. (4) with a local $\delta(4, 2) \bar{v}_{\text{xc}}(4)$.

¹Note that here we have given the equations in terms of time-ordered quantities, whereas TDDFT is usually causal. One has to pay attention to be consistent when combining the GFFT and TDDFT frameworks in practice.

²The double infinitesimals in $\chi(4, 3^{++})$ do not change the spectrum of \bar{W} , but we keep them here explicitly since they give a straightforward prescription for the contour integral in frequency space yielding E_{xc} .

Most often, $\bar{v}_{xc} \equiv v_{xc}$, the KS xc potential of TDDFT, is chosen and the resulting f_{xc} is approximated, for example, in the adiabatic local density approximation. In our derivation, \bar{f}_{xc} does not have to be a functional derivative, since it is defined by Eq. (20), which generalizes the definition of \bar{W} . This gives a rigorous foundation to attempts to use \bar{f}_{xc} other than approximate TDDFT ones in order to approximate vertex corrections to the self-energy, in particular, the so-called nanoquanta kernel and approximations to it:^{44,56–59,63–67} the only requirement is that χ_0 corresponds to the correct density. It should, however, be noted that a \bar{f}_{xc} fulfilling Eq. (20) does not necessarily exist for every χ_0 . We will give an illustration below in the Hubbard dimer.

The important message of this section is that *the exact exchange-correlation energy can be obtained with an approximate self-energy $\bar{\Sigma}_{xc}$ and with an approximate Green's function \bar{G} which is not the solution of the Dyson equation using $\bar{\Sigma}_{xc}$, but which has been chosen from the beginning. The two important requirements are consistency of the ingredients used in Eq. (25), and the fact that they stem from the real or from an auxiliary system yielding the exact density.* In the following, we will call this a *consistent scheme*, as opposed to a non-consistent scheme where different GFs are used in $E_{xc}, \bar{\Sigma}_{xc}, \bar{W}$. Here, we have shown that there is more than one possible consistent choice, which may help to design efficient approximations.

3.3 The kinetic energy

The TCTE screened self-energy $\bar{\Sigma}_{xc}$ does in general not correspond to the exact self-energy, and therefore one does not have access to the exact GF nor to the exact density matrix. As a consequence, the kinetic energy E_k cannot be computed exactly. However, with the exact Coulomb interaction energy E^{inter} at hand, this problem can in principle be overcome by using the virial theorem for the electron system^{68,69},

$$2E_k + E^{\text{inter}} = \int d^3\mathbf{r} n(\mathbf{r}) \mathbf{r} \cdot \nabla v_{\text{ext}}(r) \equiv S_{VT}. \quad (27)$$

Using the virial theorem requires in principle to know the exact density. This is not an additional requirement here, since it was already assumed throughout the above derivations. Moreover, research in the framework of DFT shows that errors induced by approximate functionals are often predominantly due to the form of the functional, whereas in many cases errors due to an approximate density are small⁷⁰. Therefore, the use of the virial theorem is a promising route to take when, as it is the case here, one can expect to access the interaction energy with good accuracy.

3.4 Comparison to the adiabatic connection

Finally, it is interesting to compare our equations to the adiabatic connection (AC) approach^{40,41,71}. In principle, this approach yields the exact full correlation energy, which encompasses correlations arising from both kinetic and Coulomb interaction energies, as well as the difference between the exchange energy calculated with the true and the KS density matrix, respectively.

Also in this approach, the correlation energy is expressed in terms of χ and χ_0 , but with an integration over a coupling constant λ that scales the Coulomb interaction and modifies v_{ext} such that the density remains constant,

$$E_c^{\text{full}} = \frac{i}{2} \int_0^1 d\lambda \int dx_1 dx_2 v_c(x_1, x_2) \left(\chi^\lambda(x_1, t_1; x_2, t_1^{++}) - \chi_0^{\text{KS}}(x_1, t_1; x_2, t_1^{++}) \right). \quad (28)$$

Since the structure of the expression is the same as that of \bar{E}_c in Eq. (17), one can express also the AC result in terms of an effective self-energy,

$$E_c^{\text{full}} = -\frac{i}{2} \int dx_1 d3 \Sigma_c^{\text{eff}}(1, 3) G^{\text{KS}}(3, 1^{++}), \quad (29)$$

where

$$\Sigma_c^{\text{eff}}(1, 3) = iG^{\text{KS}}(1, 3) \int_0^1 d\lambda \tilde{W}_{\text{pol}}^\lambda(3, 1^+), \quad (30)$$

with $\tilde{W}_{\text{pol}}^\lambda$ the polarization contribution to the λ -dependent KS TCTE screened interaction. Σ_c^{eff} is an effective correlation self-energy that contains kinetic and interaction contributions. Here, we have worked with the KS scheme, since the AC expression is often (though not always, see, e.g.,³⁸) used in the framework of KS-DFT. Analogous expressions are obtained for other allowed choices of χ_0 , e.g., stemming from a generalized KS scheme. Of course, this self-energy yields the exact full correlation energy, while it is not meant to be used in a Dyson equation to yield the GF.

It is interesting to compare the errors to be expected in practice from the AC approach on one side, and, with the errors of the approach discussed here, i.e., the combination of the calculation of E^{inter} plus the use of the virial theorem. For this estimate, we suppose the virial term S_{VT} in Eq. (27) to be known with an error that is negligible with respect to the error ΔE^{inter} stemming from approximations to χ . This is consistent with the fact that we suppose the density to be known with good accuracy. Using the virial theorem $2E_{\text{k}} + E^{\text{inter}} = S_{\text{VT}}$, the error in the kinetic energy will be $\Delta E_{\text{k}} = -\frac{\Delta E^{\text{inter}}}{2}$, leading to a total error of $\Delta E = +\frac{\Delta E^{\text{inter}}}{2}$. In the case of the AC, the error is determined entirely by the integral over response functions Eq. (28). Since the non-interacting χ_0 is subtracted, it is reasonable to suppose that the dominant contribution is linear in λ . Evidence that this is true can be found for small systems in Ref.⁷². Assuming linearity in λ , one obtains the *same* error $\Delta E = +\frac{\Delta E^{\text{inter}}}{2}$ as in our alternative scheme. Whether higher orders in λ will rather reduce or increase this result depends on whether χ_λ is convex or concave. In any case, this discussion suggests that similar errors are to be expected, while the λ -integration is avoided in the approach using the virial theorem.

3.5 Shortcomings of the TCTE self-energy

While different flavors of the TCTE screened $G\tilde{W}$ self-energies yield the exact xc energy, they will in general not yield the correct spectral function calculated from the solution of the Dyson

equation. One may expect some improvement with respect to the GW approximation for the quasiparticle (QP) energies, since the use of \bar{f}_{xc} , which is negative, reduces the polarization contribution and therefore approximates one important effect of the full vertex corrections, which is to reduce self-polarization²⁵. However, one may expect that it will not be sufficient to bring significant correction to the satellites, which are in general poorly described by the GW approximation. One reason lies in the fact that the GW self-energy is of first order in W , but used in the solution of the Dyson equation plus infinite order. Another reason is the following: the poles of the exact Green's function are the total energy differences $\pm(E_{N\pm 1,s} - E_N)$, where N is the particle number and s labels a ground ($s = 0$) or excited state s . This can be written as $\pm(E_{N\pm 1,s} - E_{N\pm 1,0}) \pm (E_{N\pm 1,0} - E_N)$, i.e., the excitation energy of the $N \pm 1$ -electron system plus the chemical potential for electrons or holes. This means that satellites of the QP, that lies at the respective chemical potential, must be found at a distance equal to the excitation energies of the $N \pm 1$ -electron system, and not, as it would be the case in the GW approximation for small systems with a discrete spectrum, at a distance close to the excitation energies of the N -electron system (plus differences in input and output QP energies when G is not calculated self-consistently). This shortcoming cannot be overcome by a $f_{xc}(\omega)$ that depends on a single frequency and multiplies $\chi(\omega)$ in frequency space: such a structure cannot shift the poles of $\chi(\omega)$. This could only be achieved by a frequency integration, as it is the case when the true three-times vertex correction is used. One should therefore at best expect corrections of the intensities of the satellites when moving from GW to $G\tilde{W}$.

4 Illustrations

In order to illustrate our main findings and suggestions, we will use a simple exactly solvable model, the symmetric Hubbard dimer^{25,73–76}. Its hamiltonian reads^{77,78}

$$\hat{H} = \sum_{i,\sigma} \epsilon_0 \hat{n}_{i\sigma} - \sum_{\langle i,j \rangle, i \neq j, \sigma} t \hat{c}_{i\sigma}^\dagger \hat{c}_{j\sigma} + U \sum_i \hat{n}_{i\uparrow} \hat{n}_{i\downarrow}. \quad (31)$$

where i, j denote the sites 1, 2, the spin $\sigma = \uparrow, \downarrow$, the external on-site potential is ϵ_0 , and t is the hopping that is linked to the kinetic energy. U is the onsite Coulomb repulsion, and $\hat{n}_{i\sigma} = \hat{c}_{i\sigma}^\dagger \hat{c}_{i\sigma}$ is the particle number operator, where \hat{c} and \hat{c}^\dagger annihilate and create a fermion, respectively. Using this simple model allows us to explore the full range of correlation, which can be quantified by the ratio U/t , and to have an unambiguous benchmark. We will use it at half filling, i.e., with two electrons, which yields non-trivial electron removal and addition features, and we will set $U = 4$ eV throughout the illustrations. One limitation of the model is the fact that the density is trivial and always exact in all methods that conserve symmetry and particle number. Since in the present work we suppose to know the exact KS ingredients, this is not a main drawback. Moreover, asymmetry in the potential removes degeneracy and therefore has a tendency to decrease correlation effects. The symmetric dimer is therefore the most critical test case. Exploring density-driven errors would be interesting, but beyond the scope of this work.

The exact analytical expressions for the time-ordered Green’s function and self-energy are given in Supporting Information. For the approximate Green’s functions we have solved the Dyson equation numerically. Our code uses retarded quantities^{79,80} which is more reliable, since the numerical results of the time-ordered calculations suffer from instabilities for some approximations in the small range of t ($t \rightarrow 0$). Computational details are given in Supporting Information.

As worked out in Subsec. 3.1, different choices for χ_0 are possible. The simplest choice is to build χ_0 with KS Green’s functions. In this case, the corresponding xc kernel f_{xc}^{KS} is the

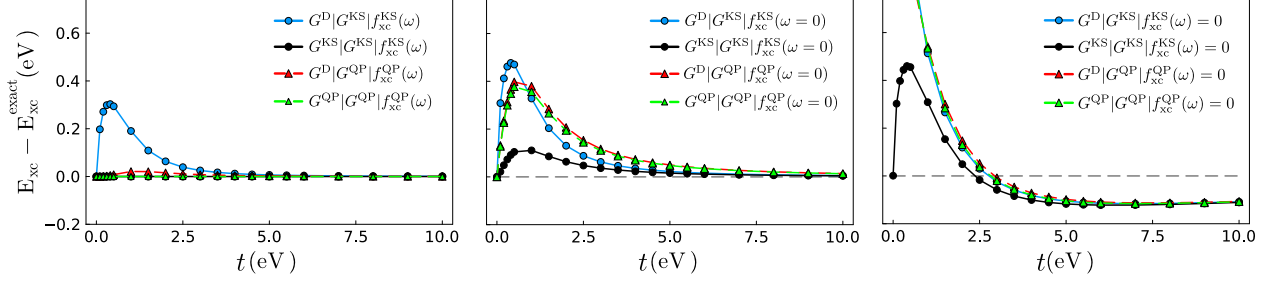


Figure 1: Symmetric Hubbard dimer at half filling and $U = 4$ eV: error of the exchange-correlation energy as a function of the hopping t . E_{xc} is obtained from $E_{xc} = -\frac{i}{2} \int G^{\text{out}} \Sigma_{xc} [G^{\text{in}}]$ for different $G^{\text{in}}, G^{\text{out}}$, which are, respectively, the input GF used to build the self-energy, and the GF that is usually the output of the Dyson equation, but for which we have more options here. Σ_{xc} is a $\tilde{G}\tilde{W}$ self-energy, built with G^{in} and using the consistently chosen xc kernel. For a compact notation, we denote this by $G^{\text{out}}|G^{\text{in}}|\bar{f}_{xc}(\omega)$. The black and sky blue solid lines with dot markers result from a self-energy built with KS ingredients and integrated, respectively, consistently with $G^{\text{out}} = G^{\text{in}} = G^{\text{KS}}$ or, inconsistently, with the $G^{\text{out}} = G^{\text{D}}$ resulting from the Dyson equation. The red and green dashed lines with triangle markers result from a self-energy built with QP ingredients and integrated, respectively, consistently with the $G^{\text{out}} = G^{\text{in}} = G^{\text{QP}}$ or, inconsistently, with the $G^{\text{out}} = G^{\text{D}}$ resulting from the Dyson equation. Left panel: results using the exact consistent $\bar{f}_{xc}(\omega)$. Middle panel: results using the adiabatic approximation $\omega = 0$ for \bar{f}_{xc} . Right panel: results obtained by neglecting \bar{f}_{xc} completely, which corresponds to a GW_0 approximation, where W_0 is calculated in the RPA and $G = G^{\text{in}}$.

one defined in TDDFT. In the symmetric Hubbard dimer the KS xc potential is a number that we set by constraining the highest occupied level (HOMO) energy of the KS system to yield the exact ionization potential. In this way we obtain the KS Green's function and χ_0^{KS} , and subsequently f_{xc}^{KS} by inversion of Eq. (20). This inversion is not unique in the symmetric Hubbard dimer, because both the exact χ and χ_0^{KS} have only one non-zero element, which is the antibonding/antibonding one (see Supporting Information). Therefore, as already pointed out in⁷⁵, only the antibonding/antibonding matrix element of the resulting f_{xc} is defined. The other elements are arbitrary, but their choice has no impact on the results, since f_{xc} appears only in the combination $\chi_0 f_{xc} \chi$.

Another natural choice would be to use the exact Green's function G to build χ_0 , since it also yields the exact density, as required. However, interestingly there is no solution to the inversion of Eq. (20) in this case. The reason is that also the bonding/bonding element of

this $\chi_0 = -iGG$ is non-vanishing. Further analysis shows that this stems from the satellite contributions to G , which are not canceled by proper vertex corrections. This is a nice illustration for one of the problems of this ill-behaved polarizability which also, for example, does not fulfill the f -sum rule⁸¹. We will instead use $\chi_0^{\text{QP}} \equiv -iG^{\text{QP}}G^{\text{QP}}$. It is built with the QP approximation G^{QP} to the exact G , where satellites are neglected and the remaining intensities normalized to 1. This can be seen as a realization of a generalized KS Green’s function, stemming from a potential that is non-local in space but instantaneous in time. Such a potential can lead to accurate QP energies⁸², but not to satellites. In a real material, the widely used hybrid functionals⁸³ fall into this class. Also many scalar long-range kernels are designed to be used on top of a χ_0^{QP} . It should again be stressed that both kernels, whether the one of the KS or the one of the QP scheme, can be called “exact”, as long as they are used consistently in conjunction with χ_0 built with the corresponding Green’s functions.

4.1 Results using exact xc kernels

In the following we will focus on the results obtained with the two kernels $f_{\text{xc}}^{\text{KS}}(\omega)$ and $f_{\text{xc}}^{\text{QP}}(\omega)$, without approximating them further. This will allow us to illustrate the effect of using an f_{xc} to simulate the full three-argument vertex of many-body perturbation theory, without further approximations.

4.1.1 Exchange-correlation energy

First, let us examine the xc contribution to the total energy, given by Eq. (25) $E_{\text{xc}} = -\frac{i}{2} \int \bar{G} \bar{\Sigma}_{\text{xc}}$. As pointed out above, here \bar{G} should *not* be the exact Green’s function nor the one resulting from the Dyson equation with $\bar{\Sigma}_{\text{xc}}$, which we will call G^{D} in the following, but \bar{G} , which is the one used to build the $G\tilde{W}$ self-energy $\bar{\Sigma}_{\text{xc}}$. This point is important since in practical applications, using G^{D} would often seem to be a natural choice, being the best available Green’s function, i.e. the one closest to the exact G . We will therefore compare

these choices in the following, by evaluating $E_{xc} = \int G^{\text{out}} \bar{\Sigma}_{xc} [G^{\text{in}}]$. Here, G^{in} is the input GF used to build the $G\bar{W}$ self-energy $\bar{\Sigma}_{xc}$, and the G^{out} is either the output of the corresponding Dyson equation G^{D} , or equal to G^{in} . In all cases, $\bar{\Sigma}_{xc}$ is built with the xc kernel \bar{f}_{xc} that is consistent with G^{in} .

For a compact notation, we use $G^{\text{out}}|G^{\text{in}}|\bar{f}_{xc}(\omega)$. For example, $G^{\text{D}}|G^{\text{KS}}|f_{xc}^{\text{KS}}(\omega)$ stands for $E_{xc} = -\frac{i}{2} \int G^{\text{D}} \Sigma_{xc} [G^{\text{KS}}]$, where the $G\bar{W}$ self-energy is built using the KS Green's function and KS xc kernel. The Dyson equation is then solved using this self-energy, and the resulting Green's function G^{D} is used in the integral. Note that while G^{D} is not the same in the KS and QP frameworks, we do not highlight this difference in the notation, since it is clear from the context. Comparison of the various flavors allows us to illustrate the importance of the consistency requirement advocated in Sec. 3.2. For subsequent investigation, we also indicate by $|\bar{f}_{xc}(\omega)$ whether the exact consistent $\bar{f}_{xc}(\omega)$ is used or further approximations are made, e.g., $|\bar{f}_{xc}(\omega = 0)$. Fig. 1 shows the difference to the exact xc energy E_{xc} . The results in the left panel were obtained using the exact consistent $\bar{f}_{xc}(\omega)$. As predicted by Eq. (25), the two consistent calculations $G^{\text{KS}}|G^{\text{KS}}|f_{xc}^{\text{KS}}(\omega)$ and $G^{\text{QP}}|G^{\text{QP}}|f_{xc}^{\text{QP}}(\omega)$ both yield the exact result. Instead, when solution of the Dyson equation is used for G^{out} we obtain $G^{\text{D}}|G^{\text{KS}}|f_{xc}^{\text{KS}}(\omega)$ and $G^{\text{D}}|G^{\text{QP}}|f_{xc}^{\text{QP}}(\omega)$, which are both inconsistent and therefore not exact. The error of the former is larger than that of the latter. This can be understood, since the difference between G^{D} and the input Green's function is larger in the case of KS than in the case of the QP input. In all cases, errors are vanishing for large t , whereas they increase in the inconsistent calculations with decreasing t . Even closer to the atomic limit, all errors tend to zero. Nevertheless, the importance of consistency is nicely illustrated by this result.

4.1.2 Kinetic energy

While an approximate self-energy used in the consistent scheme yields exact results for E_{xc} , no such scheme exists for the kinetic energy. Instead, by definition the result of the Dyson equation G^{D} is used to determine the density matrix and hence, the kinetic energy. We

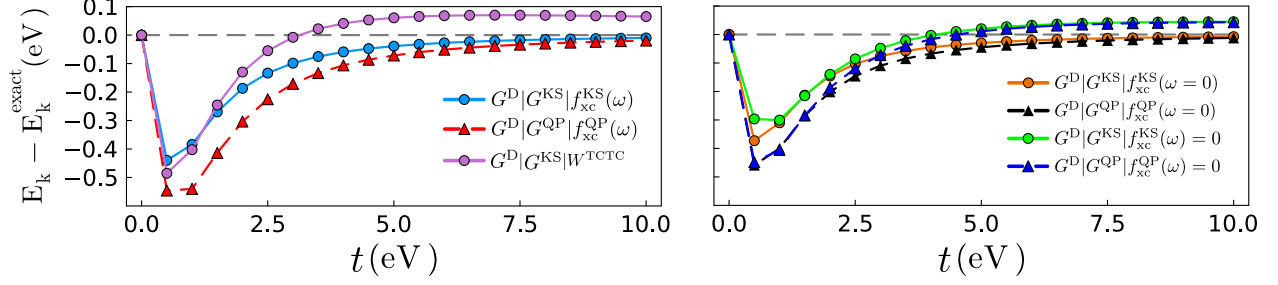


Figure 2: Kinetic energy errors as a function of the hopping parameter t . Left panel: E_k is calculated with the Green's function resulting G^D from the Dyson equation with a $G\tilde{W}$ self-energy (red with triangles and sky blue with dots) or with a $G\tilde{W}^{\text{TCTC}}$ self-energy, where W^{TCTC} is the exact TCTC screened Coulomb interaction (violet with dots). The self-energy is built with KS ingredients (sky blue and violet) or QP ingredients (red). Right panel: f_{xc} is approximated adiabatically (orange with dots for KS ingredients, black with triangles for QP ingredients) or completely neglected (green with dots for KS ingredients, dark blue with triangles for QP ingredients).

will therefore examine the error introduced by various flavors of the self-energy, starting with those that can yield the exact E_{xc} . The left panel of Fig. 2 shows the results for $G^D|G^{\text{KS}}|f_{xc}^{\text{KS}}(\omega)$ and $G^D|G^{\text{QP}}|f_{xc}^{\text{QP}}(\omega)$. Both show errors that only vanish at large t and for $t \rightarrow 0$. The KS flavor converges more quickly to the exact result with increasing t than the QP version. This favors the use of the $G\tilde{W}$ self-energy built with KS, rather than QP, ingredients. Still, the error is significant. However, as noted in Subsec. 3.3, with an exact interaction energy one can, in principle, also obtain the exact kinetic energy by using the virial theorem. This allows one to overcome the problem of not knowing the exact density matrix.

4.1.3 Spectra

The situation is different for spectral properties: here, the shortcomings of an approximate Green's function cannot be overcome easily. As for the kinetic energy, the result of the Dyson equation is used to calculate the spectra. We will explore which of the flavors of the self-energy that gives an in principle exact total energy will yield the best spectral properties, and what are the remaining problems.

Let us first look at the QP peaks of the spectral function Fig. 3 shows the error of the

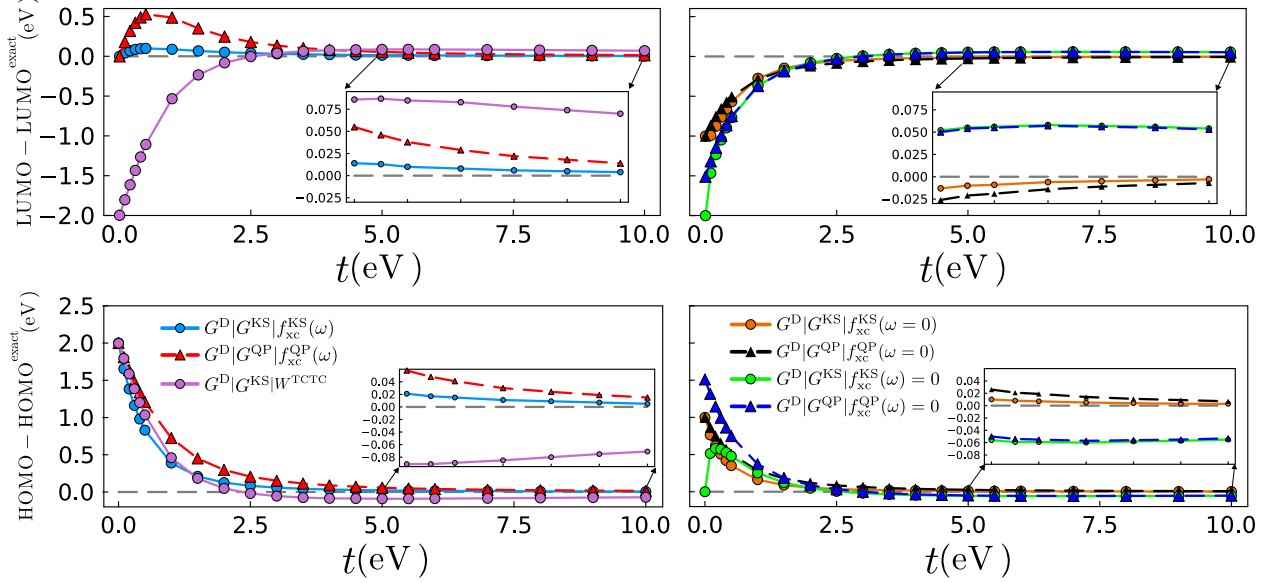


Figure 3: Error of the QP energies as a function of the hopping t . The LUMO and HOMO energy errors are shown in the upper and lower panels, respectively. Left column: The result of the Dyson equation with a $G\tilde{W}$ self-energy with KS ingredients (blue with dots) or QP ingredients (red with triangles), or with a GW self-energy using the exact TCTC screened Coulomb interaction (violet with dots) is shown. Right column: The result of the Dyson equation with a $G\tilde{W}$ self-energy with KS ingredients using a static $f_{xc}(\omega = 0)$ (orange with dots) or neglecting f_{xc} (green with dots), or with QP ingredients using a static $f_{xc}(\omega = 0)$ (black with triangles) or neglecting f_{xc} (blue with triangles) is shown.

position of the HOMO (lower panel) and of the lowest unoccupied state (LUMO) (upper panel) as a function of t . The two panels in the left column contain the HOMO and LUMO energy errors obtained with the exact KS or QP ingredients to build the $G\tilde{W}$ self-energy. While the KS and QP flavor perform very similarly for the HOMO, with small errors at larger t and a significant deviation from the exact result for small t that goes up to $U/2$ for $t \rightarrow 0$, the LUMO is relatively well described for all t , and the error vanishes for $t \rightarrow 0$. Results for the LUMO are particularly satisfying when KS ingredients are used, in which case the error does not exceed 0.1 eV for any t . For larger t , above 2.5 eV, the errors become small for both HOMO and LUMO, especially in the KS flavor, where they remain well below 0.1 eV and quickly move into the meV range (see insets).

Beyond the QP features, Fig. 4 shows the entire spectral functions for $t = 0.5$ eV. We will concentrate on the satellites. They are due to the peaks in the imaginary part of the

self-energy, which are in turn determined by the peaks of \tilde{W} : the poles of $\text{Im } \bar{\Sigma}_{\text{xc}}$ are situated at energies $\bar{\varepsilon}_i \pm \omega_j$, where $\bar{\varepsilon}_i$ is a removal/addition pole of the $G^{\text{in}} = \bar{G}$ used to build the self-energy, and ω_j is a pole of χ . Not all poles are visible in all matrix elements: in the symmetric Hubbard dimer, the bonding (antibonding) matrix element of the self-energy is dominated by the addition (removal) part of G^{in} . The bonding (antibonding) matrix element satellites are therefore found at energies higher (lower) than the LUMO (HOMO). In many real materials, all parts of the Green's function contribute to all matrix elements of the self-energy, and satellites are found on both sides of a QP. In this sense, the Hubbard dimer is an extreme case, where a given matrix element selects just one particular excitation, that may moreover not be the intuitively expected one. This does not influence our conclusions, but it is interesting to note.

The most obvious feature in Fig. 4 is the fact that satellites are not well described in general when the exact $\bar{f}_{\text{xc}}(\omega)$ is used. Their position at $\bar{\varepsilon}_i \pm \omega_j$ combines two errors: the fact that the excitation energy ω_j of the N electron system is used (see Subsec. 3.5), and the fact that $\bar{\varepsilon}_i$ can be different from the true QP energy. Since in our case the antibonding matrix element of the self-energy is dominated by the HOMO $\bar{\varepsilon}$, the exact QP energy is used in all cases studied here and the error is entirely due to the difference between the (too high) excitation energy of the N electron system with respect to the $N - 1$ electron one. For the bonding matrix element, instead, the LUMO $\bar{\varepsilon}$ is used, which is exact when QP ingredients are used, but which is too low in the KS case. This adds to the error of the (too high) excitation energy of the N electron system with respect to the $N + 1$ electron one. Since the two errors are of opposite sign, the KS ingredients yield the best result for the bonding matrix element. The difference between the N and $N \pm 1$ excitation energies should be of particular importance in finite systems, but an analogous error might also impact results in infinite systems with localized electrons.⁸⁴ Note, that the problem discussed here is different from another issue in extended systems, where the satellite position can be spoiled by the appearance of a plasmaron, a spurious solution of the QP condition that is found at some

distance from the peak in the imaginary part of the self-energy⁸⁵⁻⁸⁷. In a discrete system such as the Hubbard dimer, instead, the satellites are always found close to the position of peaks of the imaginary part of the self-energy, and the point here is that this position is calculated with the wrong number of electrons.

The biggest effect of f_{xc} is to decrease screening, which remedies the self-screening problem for the QPs^{25,88,89}, but which also decreases the satellite intensity because, as can be seen in Fig. 5, f_{xc} is always negative. Indeed, the $G\tilde{W}$ satellites in Fig. 4 are of much too weak intensity. KS ingredients do a bit better than QP ones in this respect, since in this case a weaker \bar{f}_{xc} is used (see Fig. 5), which leads to a smaller decrease of the satellite intensities, but the result is still unsatisfactory. This dilemma cannot be solved with such a simple vertex correction that is multiplicative in frequency. In other words and as expected, $G\tilde{W}$, even with exact KS or QP ingredients, cannot yield reliable satellites.

4.2 Impact of approximating f_{xc}

Understanding the impact of replacing the full vertex corrected self-energy with a $G\tilde{W}$ one is of fundamental interest. For practical applications, one also has to face the problem that the exact $f_{xc}(\omega)$ is in general not known. Therefore, we also briefly examine the impact of two widely used approximations: either a complete neglect of f_{xc} , which brings us back to the GW approximation with an RPA $W = W_0$, or at least an adiabatic approximation where only $f_{xc}(\omega = 0)$ is used, since the frequency dependence of $f_{xc}(\omega)$ is notoriously difficult to approximate. As we will see, these approximations do not have the same impact according to the flavor (KS or QP) that is chosen, and according to the combination of ingredients.

4.2.1 Exchange-correlation energy: impact of approximations

Let us first look at the quantity that is obtained exactly when $G\tilde{W}$ is used consistently, namely, the xc contribution E_{xc} to the total energy. The middle panel of Fig. 1 compares results using the adiabatic approximation $\bar{f}_{xc}(\omega = 0)$ and combining the ingredients in a

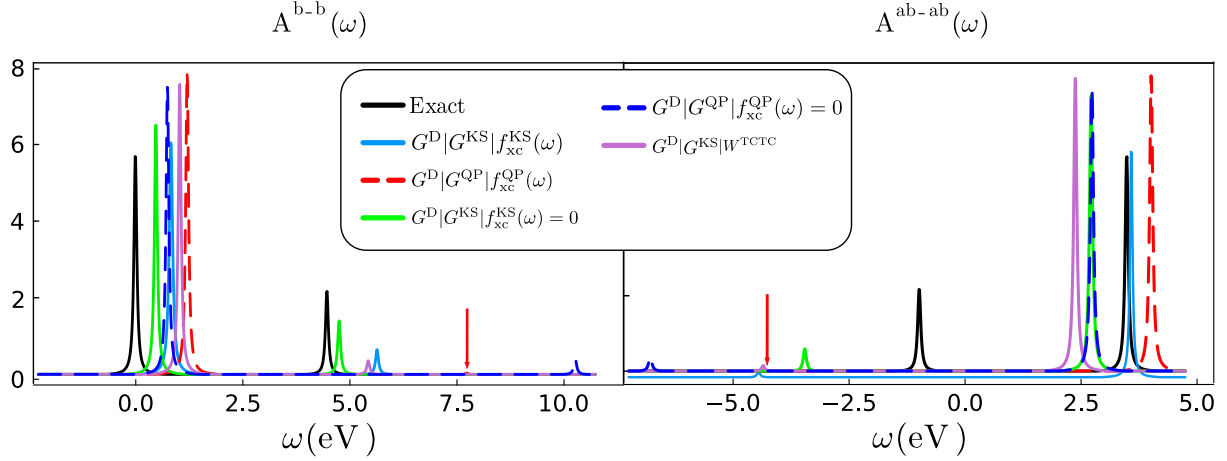


Figure 4: Bonding-bonding (left panel) and antibonding-antibonding (right panel) matrix elements of the spectral function for $U = 4$ eV and $t = 0.5$ eV. The continuous black curves are the exact result. The result of the Dyson equation using a $G\tilde{W}$ self-energy with KS ingredients and the exact f_{xc}^{KS} is in sky blue. While the result for $f_{xc}^{KS}(\omega) = 0$ is in green. The result of the Dyson equation using QP ingredients and the exact f_{xc}^{QP} is in dashed red, while the result for $f_{xc}^{QP}(\omega) = 0$ is in dashed blue. The red arrow indicates the position of the very weak satellite obtained when QP ingredients are used. Moreover, the result of the Dyson equation using a GW self-energy with the exact TCTC screening is shown in violet. The exact HOMO is situated at 0. Note that the corresponding satellites are found at higher energies. The exact QP of the LUMO is situated at 3.5 eV, with satellites in the electron removal energy range.

consistent or inconsistent way, respectively. Similarly, results in the right panel were obtained by completely neglecting f_{xc} . In all cases, the consistent results now show an error, but it is smaller than that of the corresponding inconsistent results, which demonstrates that a consistent choice of ingredients remains essential to obtain good total energies. The impact of neglecting f_{xc} is smaller when KS ingredients are used. The best results are obtained using the consistent KS flavor. When the adiabatic approximation is used, the fact that the performance of KS remains good can be explained by the fact that the quadratic frequency dependence of the kernel, which is a universal feature of f_{xc}^{90} , is milder in the KS than in the QP case, as shown in Fig. 5. Although approximate, the benefit of using f_{xc} remains very important, as can be seen by comparing the middle panel and the right panel, where results on the GW level with an RPA W_0 are given. The GW_0 results tend to the exact

result very slowly with increasing t , and a part from the consistent KS flavor, they deviate significantly from the exact result in the atomic limit. The $G^D|G^{\text{KS}}|f_{\text{xc}}(\omega) = 0$ flavor tends to $U/2$, while both consistent and non-consistent QP cases tend to $U/4$.

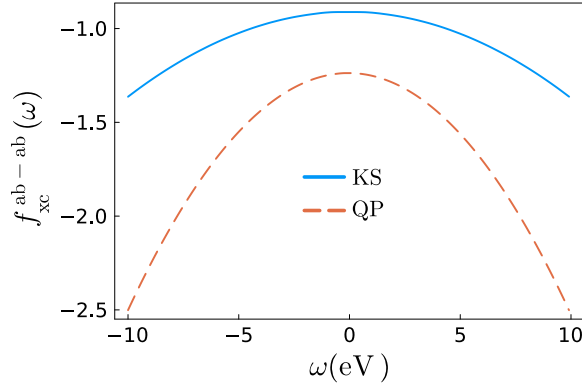


Figure 5: Antibonding matrix element of $f_{\text{xc}}(\omega)$ as a function of frequency for $U = 4$ eV and $t = 3$ eV. The light blue curve shows the xc kernel corresponding to the KS system, whereas the dashed orange result is the xc kernel that is consistent with QP ingredients.

4.2.2 Kinetic energy: impact of approximations

The kinetic energy is never exact in $G\tilde{W}$, as explained above and as illustrated in Fig. 2. The right panel of Fig. 2 also shows the impact on the kinetic energy of approximations to f_{xc} . The adiabatic approximation $f_{\text{xc}}(\omega = 0)$ has a very moderate effect, with a tendency that is rather towards improving the results. The reason for this is the fact that the kinetic energy suffers from the underestimate of the satellite intensity discussed above, which is improved when f_{xc} is weaker. Neglecting the quadratic frequency-dependence of the kernel shown in Fig. 5 is therefore rather beneficial for the kinetic energy. A complete neglect of f_{xc} , instead, spoils results in the moderate to large t -range, while further slightly improving the small- t regime, where the satellites are important. Overall, KS flavors perform slightly better than QP ones. Finally, we also show in the left panel the result of a GW^{TCTC} calculation, where the self-energy is of GW form using KS ingredients and the exact χ and therefore the exact W is used, but where the vertex $\Gamma = 1$ in the self-energy, i.e., the functional derivative in Eq. (2) is set to 1. This means that the exact test-charge test-charge (TCTC) screening is

used instead of the TCTE one that is used in the $G\tilde{W}$ approximation. Indeed, it would be tempting to think that a very good W used in GW could improve results. However, with respect to a standard GW_0 calculation using an RPA $W = W_0$, where $f_{xc} = 0$ also in χ , the results are worse, especially in the moderate to large- t regime. It has been pointed out that vertex corrections in the polarizability and in the self-energy tend to cancel partially^{47,91}: the present result is a good illustration.

4.2.3 Use of the adiabatic connection versus virial theorem

Finally, we can examine the quality of the result that can be obtained by using the virial theorem, instead of approximating the kinetic energy directly, and compare to the results obtained using the AC fluctuation-dissipation theorem discussed in Sec. 3.4. Both approaches are in principle exact, but might react differently to approximations.

Fig. 6 gives the errors of the full correlation energy including interaction and kinetic contributions, obtained using an adiabatic kernel, $f_{xc}(\omega = 0)$ and KS ingredients. In order to use the virial theorem, one has to determine the term S_{VT} in Eq. (27). We bypass the difficulty to adapt this equation to the Hubbard dimer by using the fact that here we work with the exact density in all cases, which allows us to use the exact S_{VT} , which we obtain from the exact solution as $S_{VT} \equiv 2E_k + E^{\text{inter}}$ for all values of the hopping t . The resulting S_{VT} is then used in place of the right hand side of Eq. (27) in order to obtain $E_k = (S_{VT} - E^{\text{inter}})/2$ for a given approximation to E^{inter} . This procedure gives the light blue curve (VT) in Fig. 6. As predicted in Sec. 3.4, the error is similar to the one of the AC approach using the same approximation $f_{xc}(\omega = 0)$. This is indeed due to the fact that the integrand of the full correlation energy depends approximately linearly on the coupling constant λ , as one can see in the inset of Fig. 6. The difference of the correlation energy E_c^{full} is very small around $t = 3$ eV where the behaviour is almost exactly linear, while the deviation is larger at the smaller $t = 0.5$ eV, where a quadratic λ -dependence is clearly visible. In this small- t regime, where the function is convex, the approach using the virial theorem performs better, while

also avoiding the need for the λ -integration.

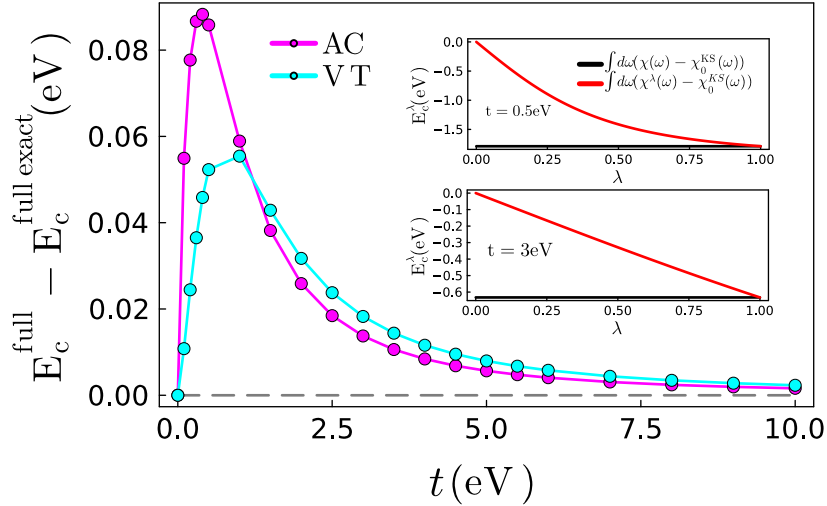


Figure 6: Error of the full correlation energy (kinetic and interaction contributions) as a function of the hopping t , when the adiabatic approximation $f_{\text{xc}}(\omega = 0)$ is made and KS ingredients are used: comparison of the adiabatic connection result (AC, in magenta) with the result obtained using the virial theorem (VT, in cyan). Insets: λ -resolved exact full correlation energy $E_c^{\text{full}} = \int_0^1 d\lambda E_c^\lambda$, evaluated within the KS scheme, as a function of λ , for $t = 0.5$ eV (upper inset) and $t = 3$ eV (lower inset).

4.2.4 Spectra

The fact that $G\tilde{W}$ does not yield the correct spectral properties cannot be overcome, but it is still interesting to examine the effect of approximations made in practice. This is done in the right panels of Fig. 3 for the QP energies, and in Fig. 4 for the satellites. For the LUMO position, both the adiabatic approximation and neglecting f_{xc} completely lead to significant worsening of the result in the small- t regime, the worst results being obtained with KS and QP GW_0 , i.e., $f_{\text{xc}} = 0$, which also slightly deteriorates results at larger t . It is interesting to note that keeping the exact $f_{\text{xc}}(\omega)$ in W alone, i.e., using the exact W^{TCTC} instead of the RPA $W = W_0$, does not fix any of these problems, as one can see in the left panel of Fig. 3 for the LUMO. The same is true also in the case of the HOMO. These findings are in line with observations on real systems⁹². Concerning the other approximations for the HOMO, shown in the lower right panel of Fig. 3, the observation concerning the GW approximation is

similar to the LUMO for moderate to large t , whereas the adiabatic approximation is rather beneficial, especially for smaller t . Also a complete neglect of f_{xc} , i.e., the GW solution with RPA $W = W_0$, decreases the error for small t , and when KS ingredients are used, the GW_0 results even reaches the correct $t \rightarrow 0$ limit. However, in this case the improvement is limited to a very small range of t close to the atomic limit. The observed trends highlight the fact that the effect of including f_{xc} is beneficial for the LUMO at all t and for the HOMO at large t , but too strong for the HOMO at small t . Since, as discussed in 4.1.3, matrix elements of the self-energy are quite particular in the Hubbard dimer, this observation should not be generalised and further analysis will be needed to eventually turn these findings into a systematic correction, which is beyond the scope of the present work.

Finally, Fig. 4 illustrates that including f_{xc} in W alone, i.e., performing a GW^{TCTC} calculation, rather worsens the satellites as compared to a GW result obtained with RPA W_0 , which illustrates again the error canceling. Therefore, in Fig. 4 the best satellite results are obtained using the GW_0 with KS ingredients and a complete neglect of \bar{f}_{xc} . Note, however, that this is not a general finding for all values of U/t .

5 Conclusions

In conclusion, the *exact* exchange-correlation contribution to the total interaction energy can be calculated using an *approximate* self-energy of the form $G\tilde{W}$. Here, \tilde{W} is a test-charge test-electron screened Coulomb interaction, which replaces the RPA or the TCTC screened interaction that are commonly used in the GW approximation. Different choices for \tilde{W} are possible, one of them being the traditionally used KS scheme, which adds an xc kernel $f_{xc}(\omega)$ from linear response TDDFT to the bare Coulomb interaction in the dielectric function. For all choices the condition is that the GF and xc kernel used to build the self-energy are consistent and yield the correct density. On top of the KS choice, we have examined the case where the GF is built with the exact QP energies. For all possible choices, it holds

that the exact xc energy is obtained by integrating the approximate self-energy with the very same GF that was used to build it. Instead, when the approximate self-energy is used in a Dyson equation and integrated with the resulting GF, the results carry an error. The importance of consistency between the GF used to build the self-energy and the GF used for the integration may explain the success of self-consistent GW total energy calculations, which indeed fulfill the requirement that the self-energy is integrated with the GF that is used to build it. Here, we show that one can obtain good quality results by being consistent without carrying out self-consistent calculations.

The exact correlation contribution to the kinetic energy cannot be accessed in the same way. Instead, we propose to use the virial theorem. We have studied the impact of widely used approximations to this approach, and compared with the use of the adiabatic connection fluctuation dissipation theorem. Our general derivation predicts that the final errors are similar, without the need of a coupling constant integration in the present approach.

Using the approximate self-energies in the Dyson equation leads to approximate GFs and therefore, to approximate spectral functions. Still, $G\tilde{W}$ yields overall better QPs than GW , and since the computational difficulty is similar, it should be preferred. The satellite problem, instead, cannot be fixed in this way.

All statements have been illustrated for the symmetric half-filled Hubbard dimer, confirming our conjectures and highlighting the fact that results obtained using KS ingredients are overall superior and less impacted by additional approximations with respect to results obtained using QP ingredients. While the Hubbard dimer is a simple model, our findings rely on derivations that are valid for the general case, and they should open the way for interesting applications to more realistic systems.

Acknowledgement

The authors acknowledge the fruitful discussions with Steffen Backes, Fabien Bruneval,

Kieron Burke and Steven Crisostomo.

This project has received funding from the European Union’s Horizon 2020 research and innovation programme under grant agreement No 800945 — NUMERICS — H2020-MSCA-COFUND-2017.

Supporting Information Available

The exact and GW solutions for the symmetric Hubbard dimer model at half-filling (two electrons) are given in literature²⁵. In this section, we provide the solutions for the model within the GW and $G\tilde{W}$ approximations using both the KS and QP flavors.

1 GW solutions

The two ingredients needed to calculate Σ_{xc} at the GW level are the GF and the screened Coulomb interaction.

1. The exact Kohn-Sham GF and the exact Quasi-Particle (QP) GF in the dimer sites basis read respectively

$$G_{ij\sigma}^{\text{KS}}(\omega) = \frac{1}{2} \left(\frac{1}{\omega - (\epsilon_0 + t - (c - U)/2) - i\eta} + \frac{(-1)^{i-j}}{\omega - (\epsilon_0 + 3t - (c - U)/2) + i\eta} \right), \quad (32)$$

$$G_{ij\sigma}^{\text{QP}}(\omega) = \frac{1}{2} \left(\frac{1}{\omega - (\epsilon_0 + t - (c - U)/2) - i\eta} + \frac{(-1)^{i-j}}{\omega - (\epsilon_0 - t + (c + U)/2) + i\eta} \right), \quad (33)$$

where $c = \sqrt{16t^2 + U^2}$. The KS GF (G^{KS}) is obtained by introducing an energy shift to the poles of the non-interacting GF such that HOMO energy becomes exact⁹³. The QP GF (G^{QP}) equals the exact GF without the satellite contributions and with the quasiparticle intensities set to 1.

2. We use both the exact screened Coulomb interaction W and approximations denoted W_0^{KS} or W_0^{QP} , depending on the choice of the GF used to compute the polarizability.

The W_0^{KS} and W_0^{QP} are calculated within the Random Phase Approximation (RPA), using the following irreducible polarizabilities

$$P_{\text{RPA}}^{\text{KS}}(1, 2) = -iG^{\text{KS}}(1, 2^+)G^{\text{KS}}(2, 1^+), \quad (34)$$

and

$$P_{\text{RPA}}^{\text{QP}}(1, 2) = -iG^{\text{QP}}(1, 2^+)G^{\text{QP}}(2, 1^+), \quad (35)$$

respectively for the KS and QP cases. They have the following analytical expressions

$$P_{\text{RPA},ij\sigma}^{\text{KS}}(\omega) = \frac{(-1)^{i-j}}{4} \left(\frac{1}{\omega - 2t + i\eta} - \frac{1}{\omega + 2t - i\eta} \right), \quad (36)$$

$$P_{\text{RPA},ij\sigma}^{\text{QP}}(\omega) = \frac{(-1)^{i-j}}{4} \left(\frac{1}{\omega + (2t - c) + i\eta} - \frac{1}{\omega - (2t - c) - i\eta} \right). \quad (37)$$

For the exact W , we use the exact reducible polarizability χ , which is related to the 2-particle Green's Function (G_2)

$$\chi(1, 2) = -iG(1, 1^+)G(2, 2^+) + iG_2(1, 2, 1^+, 2^+), \quad (38)$$

where G_2 is the 2-GF. In the Hubbard dimer site (ij) basis we have

$$\begin{aligned} \chi_{ij\sigma_1\sigma_2}(\omega) = \sum_{s \neq 0} \left[\langle N_0 | \hat{c}_{i\sigma_1}^\dagger \hat{c}_{i\sigma_1} | N_s \rangle \langle N_s | \hat{c}_{j\sigma_2}^\dagger \hat{c}_{j\sigma_2} | N_0 \rangle \frac{1}{\omega + (E_0^N - E_s^N) + i\eta} \right. \\ \left. - \langle N_0 | \hat{c}_{j\sigma_2}^\dagger \hat{c}_{j\sigma_2} | N_s \rangle \langle N_s | \hat{c}_{i\sigma_1}^\dagger \hat{c}_{i\sigma_1} | N_0 \rangle \frac{1}{\omega - (E_0^N - E_s^N) - i\eta} \right], \quad (39) \end{aligned}$$

which leads to the following solutions

$$\begin{aligned} \chi_{ij\uparrow\uparrow}(\omega) = \frac{(-1)^{i-j}}{2a^2} \left(\frac{1}{\omega - (c + U)/2 + i\eta} - \frac{1}{\omega + (c + U)/2 - i\eta} \right) \\ + (-1)^{i-j} \frac{16t^2}{2a^2(c - U)^2} \left(\frac{1}{\omega - (c - U)/2 + i\eta} - \frac{1}{\omega + (c - U)/2 - i\eta} \right), \quad (40) \end{aligned}$$

$$\begin{aligned} \chi_{ij\uparrow\downarrow}(\omega) = & \frac{(-1)^{i-j}}{2a^2} \left(\frac{1}{\omega - (c+U)/2 + i\eta} - \frac{1}{\omega + (c+U)/2 - i\eta} \right) \\ & - (-1)^{i-j} \frac{16t^2}{2a^2(c-U)^2} \left(\frac{1}{\omega - (c-U)/2 + i\eta} - \frac{1}{\omega + (c-U)/2 - i\eta} \right), \end{aligned} \quad (41)$$

where $a^2 = 2 \left(\frac{16t^2}{(c-U)^2} + 1 \right)$ and $\chi_{ij\uparrow\uparrow} = \chi_{ij\downarrow\downarrow}$, $\chi_{ij\uparrow\downarrow} = \chi_{ij\downarrow\uparrow}$.

The spin-independent χ matrix in the site basis is a sum over spins, i.e. $\chi_{ij}(\omega) = \chi_{ij\uparrow\uparrow} + \chi_{ij\uparrow\downarrow} + \chi_{ij\downarrow\uparrow} + \chi_{ij\downarrow\downarrow}$. In the bonding and anti-bonding (b/ab) basis, χ reads

$$\begin{pmatrix} 0 & 0 \\ 0 & \chi_{\text{ab-ab}}(\omega) \end{pmatrix}, \quad (42)$$

where $\chi_{\text{ab-ab}}(\omega) = 2(\chi_{11}(\omega) + \chi_{22}(\omega))$. We can now write the screened Coulomb interaction W in the different flavors. The exact screened Coulomb interaction is

$$\begin{aligned} W(1, 2) &= v_c(1, 2) + \int d(34) v_c(1, 3) P(3, 4) W(4, 2), \\ &= v_c(1, 2) + \int d(34) v_c(1, 3) \chi(3, 4) v_c(4, 2), \end{aligned}$$

or, in the site basis

$$\begin{aligned} W_{ij}(\omega) &= U\delta_{ij} + U \sum_{k\sigma} P_{ik\sigma}(\omega) W_{kj}(\omega), \\ &= U\delta_{ij} + U^2 \sum_{\sigma\sigma'=\uparrow,\downarrow} \chi_{ij\sigma\sigma'}(\omega), \end{aligned}$$

which leads to

$$W_{ij}(\omega) = U\delta_{ij} + (-1)^{i-j} \frac{2U^2}{a^2} \left(\frac{1}{\omega - (c+U)/2 + i\eta} - \frac{1}{\omega + (c+U)/2 - i\eta} \right).$$

By using Eq.s (36)(37), we find

$$W_{0,ij}^{\text{KS}}(\omega) = U\delta_{ij} + (-1)^{i-j} \frac{U^2 t}{h} \left(\frac{1}{\omega - h + i\eta} - \frac{1}{\omega + h - i\eta} \right), \quad (43)$$

where $h = \sqrt{4t^2 + 4Ut}$, and

$$W_{0,ij}^{\text{QP}}(\omega) = U\delta_{ij} + (-1)^{i-j} \frac{U^2(c/2 - t)}{h'} \left(\frac{1}{\omega - h' + i\eta} - \frac{1}{\omega + h' - i\eta} \right), \quad (44)$$

where $h' = \sqrt{(2t - c)^2 + 4U(c/2 - t)}$. Now, by using G^{KS} , G^{QP} , W_0^{KS} , W_0^{QP} and W we calculate the different flavors of Σ_{xc} by integrating in frequency space. Finally, we convert Σ_{xc} in Eq. (23) to frequency space. Note that the use of multiple infinitesimals in Eq. (23) is not important for the self-energy itself, but for the calculation of E_{xc} , as the respective weight of the infinitesimals in the different contributions indicates the contour that is to be used in the integral. So

$$\Sigma_{\text{xc},ij\sigma}(\omega) = \frac{i}{2\pi} \int d\omega' G_{0,ij\sigma}(\omega' + \omega) W_{0,ji}(\omega') e^{3i\omega'\eta}, \quad (45)$$

where G_0 can be G^{KS} or G^{QP} , and W_0 can be W_0^{KS} , W_0^{QP} or W .

The solutions of the different GW flavors are

$$\Sigma_{\text{xc},ij\sigma}^{G^{\text{KS}}W_0^{\text{KS}}}(\omega) = -\frac{U}{2}\delta_{ij} + \frac{U^2 t}{2h} \left(\frac{1}{\omega - (\epsilon_0 + 3t - (c - U)/2 + h) + i\eta} + \frac{(-1)^{i-j} e^{-3i\omega\eta}}{\omega - (\epsilon_0 + t - (c - U)/2 - h) - i\eta} \right), \quad (46)$$

$$\Sigma_{\text{xc},ij\sigma}^{G^{\text{KS}}W}(\omega) = -\frac{U}{2}\delta_{ij} + \frac{U^2}{a^2} \left(\frac{1}{\omega - (\epsilon_0 + 3t + U) + i\eta} + \frac{(-1)^{i-j} e^{-3i\omega\eta}}{\omega - (\epsilon_0 + t - c) - i\eta} \right), \quad (47)$$

$$\Sigma_{\text{xc},ij\sigma}^{G\text{QP}W_0^{\text{QP}}} = -\frac{U}{2}\delta_{ij} + \frac{U^2(\frac{c}{2} - t)}{2h'} \left(\frac{1}{\omega - (\epsilon_0 - t + (c + U)/2 + h') + i\eta} + \frac{(-1)^{i-j}e^{-3i\omega\eta}}{\omega - (\epsilon_0 + t - (c - U)/2 - h') - i\eta} \right), \quad (48)$$

and,

$$\Sigma_{\text{xc},ij\sigma}^{G\text{QP}W} = -\frac{U}{2}\delta_{ij} + \frac{U^2}{a^2} \left(\frac{1}{\omega - (\epsilon_0 - t + c + U) + i\eta} + \frac{(-1)^{i-j}e^{-3i\omega\eta}}{\omega - (\epsilon_0 + t - c) - i\eta} \right). \quad (49)$$

The non-interacting $\chi_0(1, 2) = -iG(1, 2^+)G(2, 1^+)$ does not have the same structure as the exact χ for the Hubbard dimer, when G is the exact GF. In fact,

$$\begin{aligned} \chi_{0,ij}^{GG}(\omega) = & (-1)^{i-j} \frac{(1 + \frac{4t}{c-U})^4}{2a^4} \times \left(\frac{1}{\omega + 2t - c + 2i\eta} - \frac{1}{\omega - 2t + c - 2i\eta} \right) + \\ & \frac{(1 + \frac{4t}{c-U})^2(1 - \frac{4t}{c-U})^2}{a^4} \times \left(\frac{1}{\omega - c + 2i\eta} - \frac{1}{\omega + c - 2i\eta} \right) \\ & + (-1)^{i-j} \frac{(1 - \frac{4t}{c-U})^4}{2a^4} \times \left(\frac{1}{\omega - 2t - c + 2i\eta} - \frac{1}{\omega + 2t + c - 2i\eta} \right), \quad (50) \end{aligned}$$

which yields, in the b/a-b basis

$$\chi_0^{GG}(\omega) = \begin{pmatrix} 2C_2 & 0 \\ 0 & 2C_1 + 2C_3 \end{pmatrix}, \quad (51)$$

where C_1 , C_2 and C_3 correspond to the first, second and last term in Eq. 50, respectively. The fact that the bonding-bonding matrix element does not vanish, contrary to the exact interacting χ Eq. 42, explains why no f_{xc} can be found that would link χ_0^{GG} and χ in a Dyson equation.

2 $G\tilde{W}$ solutions

The test-charge test-electron screened interaction is defined as

$$\tilde{W}(1, 2) = v_c(1, 2) + \int d(34) \left(v_c(1, 3) + f_{xc}(1, 3) \right) \chi(4, 2) v_c(4, 2). \quad (52)$$

The two f_{xc} kernels that we used in the main text are given by the matrix equations below

$$f_{xc}^{\text{KS}}(\omega) = [\chi_0^{\text{KS}}(\omega)]^{-1} - [\chi(\omega)]^{-1} - v_c, \quad (53)$$

$$f_{xc}^{\text{QP}}(\omega) = [\chi_0^{\text{QP}}(\omega)]^{-1} - [\chi(\omega)]^{-1} - v_c. \quad (54)$$

In the bonding-antibonding basis, because of Eq. (42) the KS χ_0 cannot be inverted and f_{xc}^{b-b} is not determined. Instead, $f_{xc}^{\text{ab-ab}} = \frac{1}{2\chi_{0,11}} - \frac{1}{2\chi_{11}} - U$, where $\chi_{0,11}^{\text{KS}}(\omega) = \chi_{0,11\uparrow}^{\text{KS}}(\omega) + \chi_{0,11\downarrow}^{\text{KS}}(\omega)$ and $\chi_{11}(\omega) = \chi_{11\uparrow\uparrow}(\omega) + \chi_{11\uparrow\downarrow}(\omega) + \chi_{11\downarrow\uparrow}(\omega) + \chi_{11\downarrow\downarrow}(\omega)$. f_{xc}^{b-b} and $f_{xc}^{\text{ab-ab}}$ are the bonding-bonding and antibonding-antibonding elements of the f_{xc} matrix. This leads to

$$f_{xc}^{\text{KS,ab-ab}}(\omega) = \omega^2 \left(\frac{1}{4t} - \frac{a^2}{4(c+U)} \right) - t + \frac{a^2(c+U)}{16} - U, \quad (55)$$

and

$$f_{xc}^{\text{QP,ab-ab}}(\omega) = \omega^2 \left(\frac{1}{2c-4t} - \frac{a^2}{4(c+U)} \right) + 2t - c + \frac{a^2(c+U)}{16} - U, \quad (56)$$

respectively for the KS and QP cases. In the symmetric Hubbard dimer, f_{xc} does not have poles. Its frequency dependence is quadratic. Comparison of Eq. (55) with Eq. (56) shows that, since $\frac{1}{2c-4t} - \frac{a^2}{4(c+U)} > \frac{1}{4t} - \frac{a^2}{4(c+U)}$, f_{xc}^{QP} varies more strongly than f_{xc}^{KS} with ω , as it is also shown in Fig. 5.

The self-energies based on these kernels read

$$\begin{aligned} \Sigma_{\text{xc},ij\sigma}(\omega) = & i \int \frac{d\omega_1}{2\pi} G_{ij\sigma}(\omega_1 + \omega) W_{ji}(\omega_1) e^{3i\omega_1\eta} \\ & + iU \sum_{m=1,2} \int \frac{d\omega_1}{2\pi} G_{ij\sigma}(\omega_1 + \omega) f_{xcjm}(\omega_1) \chi_{mi}(\omega_1) e^{3i\omega_1\eta}, \end{aligned} \quad (57)$$

which yields

$$\begin{aligned} \Sigma_{\text{xc},ij\sigma}^{G^{\text{KS}}\tilde{W}^{\text{KS}}}(\omega) = & -\frac{U}{2}\delta_{ij} + (-1)^{i-j} \left(\frac{U}{4} - \frac{U(c+U)}{4ta^2} \right) e^{-3i\omega\eta} + \\ & \frac{U}{4a^2} \times \frac{(c+U)^2/4 - 4t^2}{t} \left(\frac{1}{\omega - (\epsilon_0 + 3t + U) + i\eta} + \frac{(-1)^{i-j} e^{-3i\omega\eta}}{\omega - (\epsilon_0 + t - c) - i\eta} \right), \end{aligned} \quad (58)$$

$$\begin{aligned} \Sigma_{\text{xc},ij\sigma}^{G^{\text{QP}}\tilde{W}^{\text{QP}}}(\omega) = & -\frac{U}{2}\delta_{ij} + (-1)^{i-j} \left(\frac{U}{4} - \frac{U(c+U)}{a^2(2c-4t)} \right) e^{-3i\omega\eta} \\ & + \frac{U}{a^2} \times \frac{(c+U)^2/4 - (2t-c)^2}{(2c-4t)} \left(\frac{1}{\omega + (\epsilon_0 - t + c + U) + i\eta} + \frac{(-1)^{i-j} e^{-3i\omega\eta}}{\omega - (\epsilon_0 + t - c) - i\eta} \right), \end{aligned} \quad (59)$$

in which \tilde{W} is the TCTE screened interaction based on the exact χ and consistent f_{xc} kernel.

When we use the the adiabatic approximation for f_{xc} to evaluate χ and Σ_{xc} , the Dyson equation becomes

$$\chi_{\text{adiab}}(\omega) = \left(\chi_0^{-1}(\omega) - f_{\text{xc}}(\omega = 0) - v_c \right)^{-1}. \quad (60)$$

We calculate two different χ_{adiab} depending on the choice of χ_0 and corresponding $f_{\text{xc}}(\omega = 0)$. So, we have $\chi_{\text{adiab}}^{\text{KS}}$ and $\chi_{\text{adiab}}^{\text{QP}}$ when χ_0^{KS} , $f_{\text{xc}}^{\text{KS}}(\omega = 0)$ and χ_0^{QP} , $f_{\text{xc}}^{\text{QP}}(\omega = 0)$ are used respectively in the equation above. This yields

$$\begin{aligned} \Sigma_{\text{xc},ij\sigma}^{G^{\text{KS}}\tilde{W}^{\text{KS}}_{\text{adiab}}}(\omega = 0) = & -\frac{U}{2}\delta_{ij} + \\ & \frac{Ut}{2\omega_1} \left(\frac{1}{\omega - (\epsilon_0 + 3t - (c-U)/2 + \omega_1) + i\eta} + \frac{(-1)^{i-j} e^{-3i\omega\eta}}{\omega - (\epsilon_0 + t - (c-U)/2) - \omega_1 - i\eta} \right), \end{aligned} \quad (61)$$

where $\omega_1 = \sqrt{4t^2 + 2t f_{\text{Hxc}}^{\text{KS}}(\omega = 0)}$, where $f_{\text{Hxc}}^{\text{KS}}(\omega = 0) = f_{\text{xc},11}^{\text{KS}}(\omega) - f_{\text{xc},12}^{\text{KS}}(\omega = 0) + 2U =$

$-2t + \frac{a^2(c+U)}{8}$ For the QP ingredients, we have, similarly

$$\begin{aligned} \Sigma_{\text{xc},ij\sigma}^{G^{\text{QP}}\tilde{W}^{\text{QP}}}(\omega=0) &= -\frac{U}{2}\delta_{ij} + \frac{U(2c-4t)}{8\omega_2} \\ &\times \left(\frac{1}{\omega - (\epsilon_0 - t + (c+U)/2 + \omega_2) + i\eta} + \frac{(-1)^{i-j}e^{-3i\omega\eta}}{\omega - (\epsilon_0 + t - (c-U/2) - \omega_2) - i\eta} \right), \end{aligned} \quad (62)$$

where $\omega_2 = \sqrt{(2t-c)^2 + (2c-4t)f_{\text{Hxc}}^{\text{QP}}(\omega=0)}$, with $f_{\text{Hxc}}^{\text{QP}}(\omega=0) = \frac{2t-c}{2} + \frac{a^2(c+U)}{16}$. Note that \tilde{W}_{adiab} is the TCTE screened interaction that includes $f_{\text{xc}}(\omega=0)$ and $\chi_{\text{adiab}}(\omega)$ within the two different schemes.

3 Total energy contributions for the Hubbard dimer

The xc and kinetic energy contributions to the total energy, given in the Galitskii-Migdal formula in Eq. (1) are written in the site basis and frequency space of the Hubbard dimer respectively as follows

$$E_{\text{xc}} = -\frac{i}{2} \sum_{ij\sigma} \int_{-\infty}^{+\infty} \frac{d\omega}{2\pi} \Sigma_{\text{xc},ij\sigma}(\omega) G_{ij\sigma}(\omega) e^{2i\omega\eta}, \quad (63)$$

$$E_{\text{k}} = it \sum_{ij,i \neq j, \sigma} \int_{-\infty}^{+\infty} \frac{d\omega}{2\pi} G_{ij\sigma}(\omega) e^{i\omega\eta}. \quad (64)$$

4 Computational details

The entire framework for this work has been developed using an in-house code, using the Julia programming language.⁹⁴ For the purpose of performing the energy integrals, we use the ‘quadgk’ library, that relies on Gauss-Kronrod quadratures.⁹⁵ Additionally, to visualize our findings effectively, we rely on the ‘Plots.jl’ library,⁹⁶ coupled with the **GR backend**. While we provide the analytic solutions and equations for the time-ordered quantities, the numerical calculations have been performed using the retarded Green’s function framework,^{79,80} which

yields numerically stable results for small t . Retarded G^R and Σ^R are obtained from the above equations with the usual sign changes of the imaginary infinitesimals. The total energy contributions defined in Eq. (63) and Eq. (66) become

$$E_{\text{xc}} = -\frac{1}{2\pi} \sum_{ij\sigma} \int_{-\infty}^{\mu} d\omega \text{Im}(\Sigma_{\text{xc},ij\sigma}^R(\omega)G_{ij\sigma}^R(\omega)), \quad (65)$$

$$E_{\text{k}} = \frac{t}{\pi} \sum_{ij,i\neq j,\sigma} \int_{-\infty}^{\mu} d\omega \text{Im}G_{ij\sigma}^R(\omega), \quad (66)$$

where μ is the chemical potential.

The code of this project, called ‘‘Symmetric Hubbard Dimer’’, is available at the following address: <https://gitlab.com/tsg1860938/symmetric-hubbard-dimer>

References

- (1) Hohenberg, P.; Kohn, W. Inhomogeneous Electron Gas. *Phys. Rev.* **1964**, *136*, B864–B871.
- (2) Gilbert, T. L. Hohenberg-Kohn theorem for nonlocal external potentials. *Phys. Rev. B* **1975**, *12*, 2111–2120.
- (3) Donnelly, R. A.; Parr, R. G. Elementary properties of an energy functional of the first-order reduced density matrix. *The Journal of Chemical Physics* **2008**, *69*, 4431–4439.
- (4) Levy, M. Universal variational functionals of electron densities, first-order density matrices, and natural spin-orbitals and solution of the $|\psi\rangle\langle\psi|$ -representability problem. *Proceedings of the National Academy of Sciences* **1979**, *76*, 6062–6065.
- (5) Martin, R.; Reining, L.; Ceperley, D. *Interacting Electrons: Theory and Computational Approaches*; Cambridge University Press, 2016.

- (6) V.M. Galitskii, A. M. Application of Quantum Field Theory Methods to the Many Body Problem. *JETP* **1950**, *7*, 96.
- (7) Kohn, W.; Sham, L. J. Self-Consistent Equations Including Exchange and Correlation Effects. *Phys. Rev.* **1965**, *140*, A1133–A1138.
- (8) Mahan, G. *Many-particle physics*; Plenum Press: New York, 1990.
- (9) Luttinger, J. M.; Ward, J. C. Ground-State Energy of a Many-Fermion System. II. *Phys. Rev.* **1960**, *118*, 1417–1427.
- (10) Klein, A. Perturbation theory for an infinite medium of fermions. II. *Phys. Rev.* **1961**, *121*, 950–956.
- (11) Holm, B. Total Energies from *GW* Calculations. *Phys. Rev. Lett.* **1999**, *83*, 788–791.
- (12) García-González, P.; Godby, R. W. Self-consistent calculation of total energies of the electron gas using many-body perturbation theory. *Phys. Rev. B* **2001**, *63*, 075112.
- (13) Caruso, F.; Rinke, P.; Ren, X.; Scheffler, M.; Rubio, A. Unified description of ground and excited states of finite systems: The self-consistent *GW* approach. *Phys. Rev. B* **2012**, *86*, 081102.
- (14) Bruneval, F.; Rodriguez-Mayorga, M.; Rinke, P.; Dvorak, M. Improved One-Shot Total Energies from the Linearized *GW* Density Matrix. *Journal of Chemical Theory and Computation* **2021**, *17*, 2126–2136, PMID: 33705127.
- (15) García-González, P.; Godby, R. W. Many-Body *GW* Calculations of Ground-State Properties: Quasi-2D Electron Systems and van der Waals Forces. *Phys. Rev. Lett.* **2002**, *88*, 056406.
- (16) Hedin, L. New Method for Calculating the One-Particle Green’s Function with Application to the Electron-Gas Problem. *Phys. Rev.* **1965**, *139*, A796–A823.

- (17) Hybertsen, M. S.; Louie, S. G. First-Principles Theory of Quasiparticles: Calculation of Band Gaps in Semiconductors and Insulators. *Phys. Rev. Lett.* **1985**, *55*, 1418–1421.
- (18) Godby, R. W.; Schlüter, M.; Sham, L. J. Trends in self-energy operators and their corresponding exchange-correlation potentials. *Phys. Rev. B* **1987**, *36*, 6497–6500.
- (19) Godby, R. W.; Schlüter, M.; Sham, L. J. Self-energy operators and exchange-correlation potentials in semiconductors. *Phys. Rev. B* **1988**, *37*, 10159–10175.
- (20) Blase, X.; Rubio, A.; Louie, S. G.; Cohen, M. L. Quasiparticle band structure of bulk hexagonal boron nitride and related systems. *Phys. Rev. B* **1995**, *51*, 6868–6875.
- (21) van Schilfgaarde, M.; Kotani, T.; Faleev, S. V. Adequacy of approximations in *GW* theory. *Phys. Rev. B* **2006**, *74*, 245125.
- (22) Kotani, T.; van Schilfgaarde, M.; Faleev, S. V. Quasiparticle self-consistent *GW* method: A basis for the independent-particle approximation. *Phys. Rev. B* **2007**, *76*, 165106.
- (23) Reining, L. The *GW* approximation: content, successes and limitations. *WIREs Computational Molecular Science* **2018**, *8*, e1344.
- (24) Bruneval, F.; Dattani, N.; van Setten, M. J. The *GW* Miracle in Many-Body Perturbation Theory for the Ionization Potential of Molecules. *Frontiers in Chemistry* **2021**, *9*.
- (25) Romaniello, P.; Guyot, S.; Reining, L. The self-energy beyond *GW*: Local and nonlocal vertex corrections. *The Journal of Chemical Physics* **2009**, *131*, 154111.
- (26) Aryasetiawan, F.; Hedin, L.; Karlsson, K. Multiple Plasmon Satellites in Na and Al Spectral Functions from Ab Initio Cumulant Expansion. *Phys. Rev. Lett.* **1996**, *77*, 2268–2271.

- (27) Guzzo, M.; Lani, G.; Sottile, F.; Romaniello, P.; Gatti, M.; Kas, J. J.; Rehr, J. J.; Silly, M. G.; Sirotti, F.; Reining, L. Valence Electron Photoemission Spectrum of Semiconductors: Ab Initio Description of Multiple Satellites. *Phys. Rev. Lett.* **2011**, *107*, 166401.
- (28) Stan, A.; Dahlen, N. E.; van Leeuwen, R. Levels of self-consistency in the GW approximation. *The Journal of Chemical Physics* **2009**, *130*, 114105.
- (29) Minnhagen, P. Aspects on diagrammatic expansion for models related to a homogeneous electron gas. *J. Phys. C: Solid State Phys.* **1975**, *8*, 1535.
- (30) Bobbert, P. A.; van Haeringen, W. Lowest-order vertex-correction contribution to the direct gap of silicon. *Phys. Rev. B* **1994**, *49*, 10326–10331.
- (31) Shirley, E. L. Self-consistent GW and higher-order calculations of electron states in metals. *Phys. Rev. B* **1996**, *54*, 7758–7764.
- (32) Grüneis, A.; Kresse, G.; Hinuma, Y.; Oba, F. Ionization Potentials of Solids: The Importance of Vertex Corrections. *Phys. Rev. Lett.* **2014**, *112*, 096401.
- (33) Hinuma, Y.; Grüneis, A.; Kresse, G.; Oba, F. Band alignment of semiconductors from density-functional theory and many-body perturbation theory. *Phys. Rev. B* **2014**, *90*, 155405.
- (34) Ren, X.; Marom, N.; Caruso, F.; Scheffler, M.; Rinke, P. Beyond the GW approximation: A second-order screened exchange correction. *Phys. Rev. B* **2015**, *92*, 081104.
- (35) Kutepov, A. L. Electronic structure of Na, K, Si, and LiF from self-consistent solution of Hedin’s equations including vertex corrections. *Phys. Rev. B* **2016**, *94*, 155101.
- (36) Kutepov, A. L. Self-consistent solution of Hedin’s equations: Semiconductors and insulators. *Phys. Rev. B* **2017**, *95*, 195120.

- (37) Pavlyukh, Y.; Uimonen, A.-M.; Stefanucci, G.; van Leeuwen, R. Vertex Corrections for Positive-Definite Spectral Functions of Simple Metals. *Phys. Rev. Lett.* **2016**, *117*, 206402.
- (38) Maggio, E.; Kresse, G. GW Vertex Corrected Calculations for Molecular Systems. *Journal of Chemical Theory and Computation* **2017**, *13*, 4765–4778, PMID: 28873298.
- (39) Wang, Y.; Ren, X. Vertex effects in describing the ionization energies of the first-row transition-metal monoxide molecules. *The Journal of Chemical Physics* **2022**, *157*, 214115.
- (40) Langreth, D.; Perdew, J. The exchange-correlation energy of a metallic surface. *Solid State Communications* **1975**, *17*, 1425–1429.
- (41) Langreth, D. C.; Perdew, J. P. Exchange-correlation energy of a metallic surface: Wave-vector analysis. *Phys. Rev. B* **1977**, *15*, 2884–2901.
- (42) Runge, E.; Gross, E. K. U. Density-Functional Theory for Time-Dependent Systems. *Phys. Rev. Lett.* **1984**, *52*, 997–1000.
- (43) Del Sole, R.; Reining, L.; Godby, R. W. $\text{GW}\Gamma$ approximation for electron self-energies in semiconductors and insulators. *Phys. Rev. B* **1994**, *49*, 8024–8028.
- (44) Reining, L.; Olevano, V.; Rubio, A.; Onida, G. Excitonic Effects in Solids Described by Time-Dependent Density-Functional Theory. *Phys. Rev. Lett.* **2002**, *88*, 066404.
- (45) Overhauser, A. W. Simplified Theory of Electron Correlations in Metals. *Phys. Rev. B* **1971**, *3*, 1888–1898.
- (46) Petrillo, C.; Sacchetti, F. Electron-gas self-energy at metallic density. *Phys. Rev. B* **1988**, *38*, 3834–3840.
- (47) Mahan, G. D.; Sernelius, B. E. Electron-electron interactions and the bandwidth of metals. *Phys. Rev. Lett.* **1989**, *62*, 2718–2720.

- (48) Hybertsen, M. S.; Louie, S. G. Electron correlation in semiconductors and insulators: Band gaps and quasiparticle energies. *Phys. Rev. B* **1986**, *34*, 5390–5413.
- (49) Hindgren, M.; Almladh, C.-O. Improved local-field corrections to the G_0W approximation in jellium: Importance of consistency relations. *Phys. Rev. B* **1997**, *56*, 12832–12839.
- (50) Schmidt, P. S.; Patrick, C. E.; Thygesen, K. S. Simple vertex correction improves GW band energies of bulk and two-dimensional crystals. *Phys. Rev. B* **2017**, *96*, 205206.
- (51) Hung, L.; da Jornada, F. H.; Souto-Casares, J.; Chelikowsky, J. R.; Louie, S. G.; Ögüt, S. Excitation spectra of aromatic molecules within a real-space GW -BSE formalism: Role of self-consistency and vertex corrections. *Phys. Rev. B* **2016**, *94*, 085125.
- (52) Olsen, T.; Patrick, C. E.; Bates, J. E.; Ruzsinszky, A.; Thygesen, K. S. Beyond the RPA and GW methods with adiabatic xc-kernels for accurate ground state and quasiparticle energies. *npj Computational Materials* **2019**, *5*, 106.
- (53) Chen, W.; Pasquarello, A. Accurate band gaps of extended systems via efficient vertex corrections in GW . *Phys. Rev. B* **2015**, *92*, 041115.
- (54) Tal, A.; Chen, W.; Pasquarello, A. Vertex function compliant with the Ward identity for quasiparticle self-consistent calculations beyond GW . *Phys. Rev. B* **2021**, *103*, L161104.
- (55) Gross, E. K. U.; Kohn, W. Local density-functional theory of frequency-dependent linear response. *Phys. Rev. Lett.* **1985**, *55*, 2850–2852.
- (56) Tokatly, I. V.; Pankratov, O. Many-Body Diagrammatic Expansion in a Kohn-Sham Basis: Implications for Time-Dependent Density Functional Theory of Excited States. *Phys. Rev. Lett.* **2001**, *86*, 2078–2081.

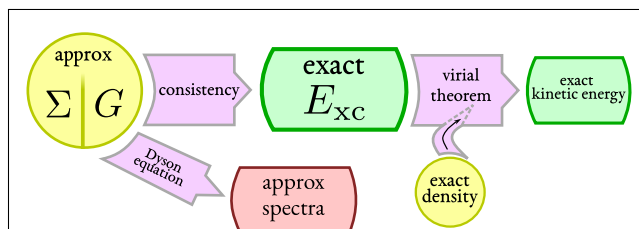
- (57) Bruneval, F.; Sottile, F.; Olevano, V.; Del Sole, R.; Reining, L. Many-Body Perturbation Theory Using the Density-Functional Concept: Beyond the *GW* Approximation. *Phys. Rev. Lett.* **2005**, *94*, 186402.
- (58) Gatti, M.; Olevano, V.; Reining, L.; Tokatly, I. V. Transforming Nonlocality into a Frequency Dependence: A Shortcut to Spectroscopy. *Phys. Rev. Lett.* **2007**, *99*, 057401.
- (59) Botti, S.; Schindlmayr, A.; Sole, R. D.; Reining, L. Time-dependent density-functional theory for extended systems. *Reports on Progress in Physics* **2007**, *70*, 357.
- (60) Singhal, S. P.; Callaway, J. Exchange correction to the dielectric function in the local exchange approximation. *Phys. Rev. B* **1976**, *14*, 2347–2351.
- (61) Hybertsen, M. S.; Louie, S. G. Ab initio static dielectric matrices from the density-functional approach. I. Formulation and application to semiconductors and insulators. *Phys. Rev. B* **1987**, *35*, 5585–5601.
- (62) Hellgren, M.; Baguet, L. Strengths and limitations of the adiabatic exact-exchange kernel for total energy calculations. *The Journal of Chemical Physics* **2023**, *158*, 184107.
- (63) Sottile, F.; Olevano, V.; Reining, L. *Phys. Rev. Lett.* **2003**, *91*, 056402.
- (64) Sharma, S.; Dewhurst, J. K.; Sanna, A.; Gross, E. K. U. Bootstrap Approximation for the Exchange-Correlation Kernel of Time-Dependent Density-Functional Theory. *Phys. Rev. Lett.* **2011**, *107*.
- (65) Adragna, G.; Del Sole, R.; Marini, A. *Phys. Rev. B* **2003**, *68*, 165108.
- (66) Marini, A.; Del Sole, R.; Rubio, A. *Phys. Rev. Lett.* **2003**, *91*, 256402.
- (67) Rigamonti, S.; Botti, S.; Veniard, V.; Draxl, C.; Reining, L.; Sottile, F. Estimating Excitonic Effects in the Absorption Spectra of Solids: Problems and Insight from a Guided Iteration Scheme. *Phys. Rev. Lett.* **2015**, *114*, 146402.

- (68) Levy, M.; Perdew, J. P. Hellmann-Feynman, virial, and scaling requisites for the exact universal density functionals. Shape of the correlation potential and diamagnetic susceptibility for atoms. *Phys. Rev. A* **1985**, *32*, 2010–2021.
- (69) Jiang, K.; Mosquera, M. A.; Oueis, Y.; Wasserman, A. Virial relations in density embedding. *International Journal of Quantum Chemistry* **2020**, *120*, e26204.
- (70) Kim, M.-C.; Sim, E.; Burke, K. Understanding and Reducing Errors in Density Functional Calculations. *Phys. Rev. Lett.* **2013**, *111*, 073003.
- (71) Ren, X.; Rinke, P.; Joas, C.; Scheffler, M. Random-phase approximation and its applications in computational chemistry and materials science. *Journal of Materials Science* **2012**, *47*, 7447.
- (72) Savin, A.; Colonna, F.; Allavena, M. Analysis of the linear response function along the adiabatic connection from the Kohn–Sham to the correlated system. *The Journal of Chemical Physics* **2001**, *115*, 6827–6833.
- (73) Romaniello, P.; Bechstedt, F.; Reining, L. Beyond the *GW* approximation: Combining correlation channels. *Phys. Rev. B* **2012**, *85*, 155131.
- (74) Carrascal, D. J.; Ferrer, J.; Smith, J. C.; Burke, K. The Hubbard dimer: a density functional case study of a many-body problem. *Journal of Physics: Condensed Matter* **2015**, *27*, 393001.
- (75) Aryasetiawan, F.; Gunnarsson, O. Exchange-correlation kernel in time-dependent density functional theory. *Phys. Rev. B* **2002**, *66*, 165119.
- (76) Coveney, C. J. N.; Tew, D. P. A Regularized Second-Order Correlation Method from Green’s Function Theory. *Journal of Chemical Theory and Computation* **2023**, *19*, 3915–3928.

- (77) J.Hubbard, Electron correlations in narrow energy bands. *Proc. R. Soc. Lond. A* **1963**, 276, 238.
- (78) J.Hubbard, Electron correlations in narrow energy bands. *Proc. R. Soc. Lond. A* **1964**, 277, 237.
- (79) Spataru, C. D.; Benedict, L. X.; Louie, S. G. Ab initio calculation of band-gap renormalization in highly excited GaAs. *Phys. Rev. B* **2004**, 69, 205204.
- (80) Honet, A.; Henrard, L.; Meunier, V. Exact and many-body perturbation solutions of the Hubbard model applied to linear chains. *AIP Advances* **2022**, 12, 035238.
- (81) Holm, B.; von Barth, U. Fully self-consistent GW self-energy of the electron gas. *Phys. Rev. B* **1998**, 57, 2108–2117.
- (82) Perdew, J. P.; Yang, W.; Burke, K.; Yang, Z.; Gross, E. K. U.; Scheffler, M.; Scuseria, G. E.; Henderson, T. M.; Zhang, I. Y.; Ruzsinszky, A.; Peng, H.; Sun, J.; Trushin, E.; Görling, A. Understanding band gaps of solids in generalized Kohn–Sham theory. *Proceedings of the National Academy of Sciences* **2017**, 114, 2801–2806.
- (83) Heyd, J.; Scuseria, G. E.; Ernzerhof, M. Hybrid functionals based on a screened Coulomb potential. *The Journal of Chemical Physics* **2003**, 118, 8207–8215.
- (84) Aryasetiawan, F.; Sakuma, R.; Karlsson, K. GW approximation with self-screening correction. *Phys. Rev. B* **2012**, 85, 035106.
- (85) Hedin, L.; Lundqvist, B.; Lundqvist, S. New structure in the single-particle spectrum of an electron gas. *Solid State Communications* **1967**, 5, 237 – 239.
- (86) Bergerse.B.; Kus, F. W.; Blomberg, C. SINGLE-PARTICLE GREENS FUNCTION IN ELECTRON-PLASMON APPROXIMATION. *Canadian J. Phys.* **1973**, 51, 102–110.

- (87) Guzzo, M.; Kas, J. J.; Sponza, L.; Giorgetti, C.; Sottile, F.; Pierucci, D.; Silly, M. G.; Sirotti, F.; Rehr, J. J.; Reining, L. Multiple satellites in materials with complex plasmon spectra: From graphite to graphene. *Phys. Rev. B* **2014**, *89*, 085425.
- (88) Nelson, W.; Bokes, P.; Rinke, P.; Godby, R. W. Self-interaction in Green's-function theory of the hydrogen atom. *Phys. Rev. A* **2007**, *75*, 032505.
- (89) Fernandez, J. J. *GW* calculations in an exactly solvable model system at different dilution regimes: The problem of the self-interaction in the correlation part. *Phys. Rev. A* **2009**, *79*, 052513.
- (90) Botti, S.; Fourreau, A.; Nguyen, F. m. c.; Renault, Y.-O.; Sottile, F.; Reining, L. Energy dependence of the exchange-correlation kernel of time-dependent density functional theory: A simple model for solids. *Phys. Rev. B* **2005**, *72*, 125203.
- (91) Minnhagen, P. Vertex correction calculations for an electron gas. *Journal of Physics C: Solid State Physics* **1974**, *7*, 3013.
- (92) Lewis, A. M.; Berkelbach, T. C. Vertex Corrections to the Polarizability Do Not Improve the *GW* Approximation for the Ionization Potential of Molecules. *Journal of Chemical Theory and Computation* **2019**, *15*, 2925–2932.
- (93) Perdew, J. P.; Norman, M. R. Electron removal energies in Kohn-Sham density-functional theory. *Phys. Rev. B* **1982**, *26*, 5445–5450.
- (94) Bezanson, J.; Edelman, A.; Karpinski, S.; Shah, V. B. Julia: A fresh approach to numerical computing. *SIAM Review* **2017**, *59*, 65–98.
- (95) Laurie, D. P. Calculation of Gauss-Kronrod Quadrature Rules. *Mathematics of Computation* **1997**, *66*, 1133–1145.
- (96) Christ, S.; Schwabeneder, D.; Rackauckas, C.; Borregaard, M. K.; Breloff, T. Plots.jl – a user extendable plotting API for the julia programming language. **2023**, *11*, 5.

TOC Graphic



The Dyson equation with an approximate self-energy leads to an approximate Green's function and to approximate spectra. However, the same approximate self-energy yields the exact exchange-correlation energy, provided the latter is evaluated following a consistent prescription.